Gas-phase Polyethylene Reactors -A Critical Review of Modelling Approaches

Rita Ferreira Alves, Tommaso Casalini, Giuseppe Storti, Timothy Mckenna

▶ To cite this version:

Gas-phase Polyethylene Reactors – A Critical Review of Modelling Approaches

Rita Ferreira Alves[a], Tommaso Casalini[b], Giuseppe Storti[b,*], Timothy F.L. McKenna[a,**]

[a]Chimie Catalyse Polymères et Procédés UMR-5265,Université de Lyon, CNRS, CPE-Lyon, UCB Lyon-1, 43 Blvd du 11 Novembre 1918, 69616 Villeurbanne Cedex, France

[b]Department of Chemistry and Applied Biosciences, Institute for Chemical and Bioengineering, ETH Zurich, Vladimir-Prelog-Weg 1-5/10, 8093 Zurich, Switzerland

*giuseppe.storti@chem.ethz.ch

**timothy.mckenna@univ-lyon1.fr

Abstract

This review looks at the different approaches to modelling the gas phase polymerization of ethylene that have been considered in the literature. It is shown that while simple, well-mixed models can give an adequate representation of the average performance of a given polymerization reactor, they do not allow one to analyze certain modelling problems such as the existence of temperature gradients or particle segregation, nor can they be used to treat operational modes such as condensed cooling where there can be up to three different phases in different parts of the reactor. For this, more complex models are required. These can take the form of compartmentalized models or even models based on computation fluid dynamics. However, long computational times can be required to fully exploit these models. Furthermore, significant progress needs to be made if we are to address important phenomena such as agglomeration or particle attrition during polymerization.

1 Introduction

Polyethylene (PE) is the most common thermoplastic in the world, with current annual on-line capacity reaching over 100 million tonnes. Industrial processes for polyethylene (PE) production can be divided into different categories according to the phase in which the

polymerization takes place: solution, slurry or gas-phase processes, with the latter two being more significant in terms of production volumes. While slurry phase processes are commercially important for high density polyethylene (HDPE), gas-phase processes were responsible for 40% of the total PE production in 2018, meaning that is the most widely used process. Due to their versatility, gas-phase processes can be used to make products with a full range of densities, from linear low density polyethylene (LLDPE) to high density polyethylene (HDPE) in the same reactor [1][2]. Up until recently, all PE plants operated fluidized bed reactors (FBR), since this was the only reactor configuration that allowed enough heat evacuation in order to achieve commercially pertinent rates of polymerization [1]–[3]. However, as of 2017 a new PE plant has been under construction with a new reactor configuration. This novel process, termed Hyperzone, is made of a FBR reactor followed by a multi-zone circulating reactor (MZCR) to make bimodal HDPE. In the MZCR, one can observe two distinct hydrodynamic zones. Thus, the growing polymer is kept in continuous circulation between "fast fluidization" and "packed bed" zones [4]. Nevertheless, virtually all other plants use FBRs for their gas phase polymerization, and so the focus of this review will be exclusively on this type of reactor.

A diagram of a typical FBR for PE production is shown in Figure 1. This scheme is based on the Unipol process, but other processes (such as Spherilene) are licensed worldwide [3].
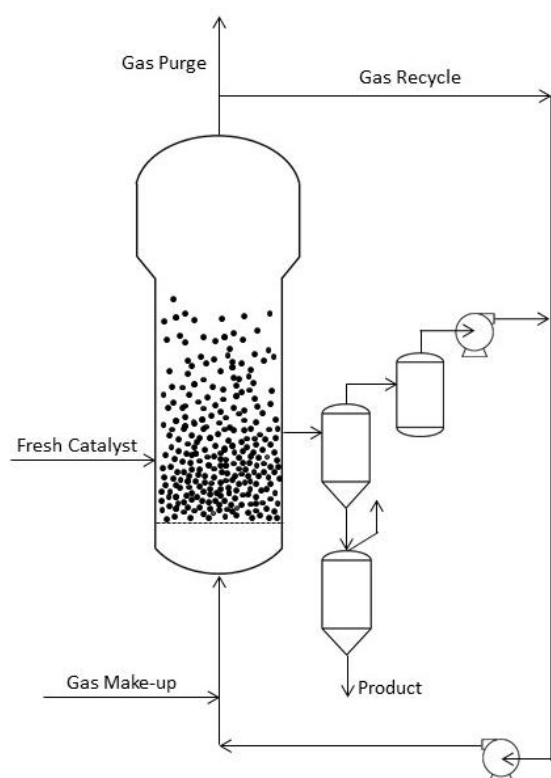
Figure 1. Scheme of typical fluidized bed reactor.

The reactor is essentially an empty cylinder with an expansion zone at the top (to reduce the gas velocity and help prevent any fine particles from flowing out of the reactor and into the recycle compressor), and a distributor plate at the bottom. Heterogeneous Ziegler-Natta or metallocene catalyst (or prepolymerized catalyst) particles are continually introduced into the reactor, ready to react with the fresh monomer(s) being fed at the bottom of the bed. Active species diffuse to the particle, through the pores, and then into and through polymer covering the active sites. The highly exothermic polymerization occurs at the active sites (see section 2.1). Continual accumulation of polymer causes the particles to grow from an original diameter on the order of 10-50 microns to a diameter of several hundred microns when they are removed through a product discharge valve. From there, they go into a series of degassing tanks to separate the unreacted monomers. The gaseous recycle stream is compressed, cooled and afterwards mixed with fresh monomers, hydrogen and eventually other compounds, then fed back into the reactor.

Typical reactor dimensions and operating conditions can be found in Table 1:

Table 1. Typical reactor dimensions and operating conditions.

Parameter	Range
Reactor Height (m)	10-16
Reactor Diameter (m)	2.5-4
Temperature (ºC)	70-110
Pressure (bar)	20-25
Per Pass Conversion (%)	2 – 30

Over the years, advances in catalyst technology have made it possible to produce several kilograms of polymer per gram of supported catalyst. Heat transfer can be a challenge because as the space time yield of the bed improves due faster polymerization, the quantity of heat that needs to be removed increases proportionally. The principal means of removing the heat generated by polymerization is convective heat transfer between solid particles and the gas phase. FBRs are the best option for maximizing heat transfer, as the gas flows through the bed at reasonably high speed (between 0.5 and 1m/s), much higher than in stirred beds. Of course, convective heat transfer improves as the relative gas-particle velocities improve, but this is not a parameter that one can choose arbitrarily. If the velocity is too low, the bed will not be

fluidized, but if the velocity is too high the particles will be blown out of the bed, which can cause problems downstream. Another option to relieve the reactor of excessive heat is to manipulate the inlet gas temperature, but this is also limited because one cannot have very large temperature gradients in the reactor either. Perhaps the most common way of improving the heat removal from the reactor is to alter the physical nature of the feed stream. Chemically inert compounds such as ethane or higher alkanes can be introduced into the reactor in the place of nitrogen to increase the heat capacity of the gas stream [1], [5], [6]. When these alkanes are added as uncondensed vapors, the reactor is working under what is called "super dry mode".

Even more heat can be removed when these compounds are (partially) condensed in the feed stream. When this happens, the FBR is said to be operating in "condensed mode". In this case the recycle stream is compressed, and then cooled by passing it through at least one external heat exchanger to a temperature below that of the dew point of the gas mixture. The resulting stream is then fed into the lower zone of the reactor in such a way that the liquid is sprayed into the reacting zone, and the droplets of liquid are vaporized by the heat of reaction [5]. Alkanes such as isomers of butane, pentane or hexane are most commonly used to this end. In the case of super dry mode, or condensed mode, the added inert alkanes can be referred to as induced condensing agents (ICA). Monomers such as 1-butene or 1-hexene can also be liquefied and contribute to energy evacuation as well. In normal condensed mode, it has been shown that the liquid droplets evaporate rapidly, and that the clear majority of the powder bed in a typical reactor contains only solid particles and a continuous gas phase [7], [8]. On the other hand, adding an ICA has a much more significant effect on the observed rate of polymerization that cannot be exclusively explained by better heat evacuation. It turns out that the well-known co-solubility effect implies that the concentration of ethylene in the polymer amorphous phase is increased by the presence of a heavier hydrocarbons [9]–[13]. However, only very recently has this effect been taken into consideration in the development of processes models.

Given the importance of the gas-phase production of PE, significant efforts have been made to model this process over the years. As it has been discussed many times, modelling a complex chemical process such as this involves integrating models that describe physical and chemical phenomena that are occurring over numerous different length and time scales; from the active site on the supported catalyst surface all the way up to the complex flow patterns in a bubbling FBR. In order to better frame the problem, it is useful to implement a multiscale

approach as shown schematically in Figure 2 [1], [14]–[16]. The three length scales we choose to define here are:

- microscale – Polymerization kinetics;
- mesoscale – Particle morphology, thermodynamics (including sorption and diffusion), intraparticle mass and heat transfer;
- macroscale – Mixing, overall mass and heat balances, particle population balances, residence time distribution.

In a multiscale approach, each phenomenon should be appropriately modelled at its specific level. The relevant information is then transmitted to the models at other scales.
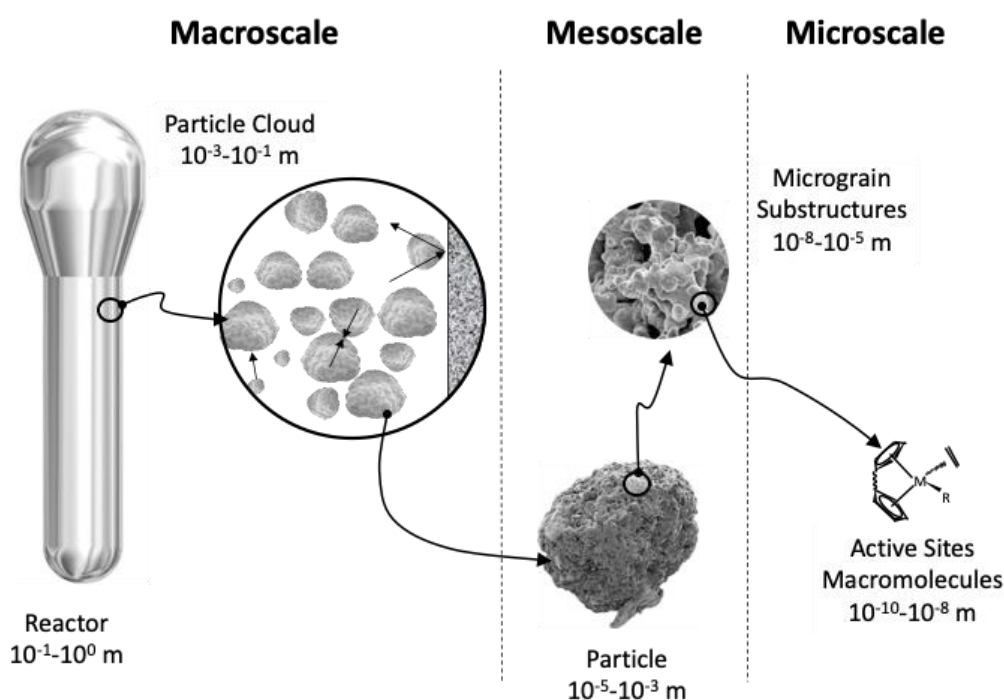
Figure 2. Possible different length scales to be considered for reactor modelling. © 2012 Wiley-VCH Verlag & Co. KGaA, Boschstr. 12, 69469 Weinheim, Germany. Reproduced with permission.

A few authors have already published reviews to guide us through the different modelling approaches in gas phase polyolefin polymerization. For instance Xie *et al*. [17], Kiparissides [18], and Hamielec and Soares [19] discussed the catalysts used and reaction kinetics, as well as the main mathematical models available at the time the articles were written. Xie *et al*. [17]

and Kiparissides [18] focused on the reactor modelling, while Hamielec and Soares [19] concentrated on mathematical modelling of the polymerization kinetics and polymer properties. Nevertheless, all of these papers, either implicitly or explicitly involve the concept of multiscale models. Abbasi *et al.* [15] and Zhu *et al.* [16] explicitly invoked the need for multiscale models for gas phase olefin polymerization. While the latter group focused on polypropylene rather than PE and defined 5 scales rather than the 3 proposed above, they made it clear that regardless of the model one chose for the reactor scale, intraparticle gradients of heat and mass transfer will influence how the particles behave in the reactor. Sun *et al.* [20] looked more at mesoscale phenomena in FBRs, compared different types of Computational Fluid Dynamics (CFD) and Discrete Element Method (DEM) modelling approaches for PE and clearly demonstrated that mesoscale and macroscale phenomena are connected. Kaneko *et al.* [21] also used a DEM-based approach to demonstrate the interaction between macroscale mixing and mesoscale particle overheating. There are of course many other studies in the open literature that support this multiscale concept (either implicitly or explicitly), that might use different numerical approaches and assumptions, but they all show the fact that the more a model takes into account the interaction between phenomena occurring at different scales, the more information one can obtain from it. Of course, important questions to ask at this point include "how much information do we want from our model?"; and "which model should we choose?" The main purpose of this review is to attempt to answer this last question rather than to present an exhaustive review of all of the modelling papers in the literature. Furthermore, in order to move forward with future modelling studies, it is also important to identify what information is still lacking for us to be able to write and solve comprehensive, *a priori* models of ethylene polymerization in fluidized bed reactors. However, given the complexity of the interactions between the phenomena that occur at different length scales in the reactor, it is useful to quickly review the micro- and mesoscale models currently used for heterogeneously catalyzed ethylene polymerization.

2   Micro- and mesoscale modelling

While microscale kinetics is not the focus of this review, it is important to point out once again that, in order to understand the relationship between the different length scales in the reactor and the polymer properties, it is necessary to understand what levels of accuracy might be required to have confidence in a full reactor model. For instance, if the microscale model is

poorly defined and missing important parameters, is it really useful to develop a highly detailed reactor model to predict the impact of residence time distribution changes on the molecular weight distribution? It is therefore useful to think about the importance of the microscale even if we are primarily interested in the macroscale. Similarly, for the mesoscale – if we cannot describe heat and mass transfer to and from the active sites, how good will our macroscale model be? We will therefore do a quick overview of the microscale (reaction kinetics) and mesoscale (particle growth and morphology, heat and mass transfer between phases and system thermodynamics) before turning our attention to macroscale modelling.

McKenna and Soares (2001) [22] reviewed the available single particle models for olefins polymerization on supported catalysts. The authors paid particular attention to particle growth, polymerization rate, concentration and temperature radial profiles and particle microstructure and morphology. They also suggested that models available at the time were able to fit experimental observations (even if they did so by treating diffusion, heat transfer, mass transfer and kinetic coefficients as adjustable parameters), and therefore at least partially explain the relationship between reactor conditions and observed properties. However this, and later reviews [23][24], also showed that these models have inherent shortcomings that are also linked to the inability to predict particle morphology in a reasonable manner. Progress needs to be made in this direction, but it also appears that overcomplicating particle models will not necessarily improve their predictive capabilities and might even diminish our ability to use them to predict reactor behaviour [22]. Soares [25] also reviewed the efforts made in the field of mathematical modelling of the microstructures of polyolefins made by coordination polymerizations. Finally, Touloupidis [14] reviewed the multiscale polymerization process modeling framework, focusing on polymerization kinetics.

2.1   Microscale Modeling

Commercial gas-phase ethylene polymerization used supported catalysts, such as Ziegler–Natta, chromium oxides, and supported metallocene. Table 2 illustrates some of the elementary reactions considered for a kinetic model of ethylene copolymerization, where monomer 1 is ethylene and monomer 2 the co-monomer, and terminal copolymerization model is considered. The superscript "k" specifies the type of catalytic site. In the case of an ideal metallocene or other single-site catalyst, k =1. For Ziegler-Natta or Chromium oxide catalysts, there is no defined value for k. For Ziegler-Natta catalysts it is typically between 3

and 5, whereas for chromium catalysts, it can be much higher (see reference [26] for a discussion on the difference between single and multiple site catalysts). The kinetic constants (k) are assumed to follow Arrhenius law (Eq.(1)) [27], where k_0 is the pre-exponential constant, E_a is the activation energy, R is the universal gas constant and T is the absolute temperature. The nature of the active sites is considered unchangeable once they are activated (in other words the propensity of the sites to propagate, terminate, transfer, etc. is always the same when the sites are active).

$$k = k_0 \exp\left(-\frac{E_a}{RT}\right) \tag{1}$$

Table 2. Main reaction steps in the copolymerization of ethylene [27]

Site Activation $$S_p^k + AlR_3 \xrightarrow{k_a^k} P_0^k$$		Conversion of inactive potential catalyst sites, S_p^k, to reactive vacant sites, P_0^k. Activation commonly occurs by reaction of a potential site with a cocatalyst (AlR_3).
Chain initiation $$P_0^k + M_i \xrightarrow{k_{0i}^k} P_{1,i}^k$$		A monomer molecule of type i, M_i, reacts with an activated vacant site, producing an active site occupied by a chain made of a single monomer, $P_{1,i}^k$.
Chain Propagation $$P_{n,1}^k + M_i \xrightarrow{k_{p1i}^k} P_{n+1,i}^k$$ $$P_{n,2}^k + M_i \xrightarrow{k_{p2i}^k} P_{n+1,i}^k$$		Main polymerization reaction step. The active chain of length n and with a monomer of type j at the active site, $P_{n,j}^k$, reacts with a monomer molecule of type i, increasing its chain length by one, $P_{n+1,i}^k$.
Chain Transfer		These reactions terminate the growth of live polymer chains, forming dead polymer chains, D_n^k, and vacant active sites, P_0^k, or $P_{1,j}^k$. Termination by hydrogen is thought to lead to a dormant site P_H^k.
To hydrogen	$P_{n,i}^k + H_2 \xrightarrow{k_{trH,i}^k} P_H^k + D_n^k$	
To co-catalyst	$P_{n,i}^k + A \xrightarrow{k_{trA,i}^k} P_0^k + D_n^k$	
To monomer	$P_{n,i}^k + M_j \xrightarrow{k_{trj,i}^k} P_{1,j}^k + D_n^k$	
Spontaneous	$P_{n,i}^k \xrightarrow{k_{trSP,i}^k} P_0^k + D_n^k$	
Dormant Site Reactivation $$P_H^k + M_i \xrightarrow{k_{Hi}^k} P_{1,i}^k$$		A monomer molecule, M_i, reacts with a dormant site, producing an active site occupied by a single monomer, $P_{1,i}^k$. The

Site Deactivation		Deactivation reactions form dead sites, C_D^k and dead polymer chains. Typically, spontaneous deactivation predominates, but deactivation by other means, such as poisoning reactions with polar impurities present in the reactor, is also possible.
By hydrogen	$P_{n,i}^k + H_2 \xrightarrow{k_{trH,i}^k} C_D^k + D_n^k$	
By co-catalyst	$P_{n,i}^k + A \xrightarrow{k_{trA,i}^k} C_D^k + D_n^k$	
By monomer	$P_{n,i}^k + M_j \xrightarrow{k_{tri,j}^k} C_D^k + D_n^k$	
Spontaneous	$P_{n,i}^k \xrightarrow{k_{trSP,i}^k} C_D^k + D_n^k$	

In certain circumstances, simplified versions of the kinetic scheme shown in Table 2 are used, and the degree of simplification that is acceptable depends on the type of information required. While seemingly obvious, this last statement can be applied at virtually every level of reactor modelling and thought needs to be given to what exactly we know and what exactly we hope to learn from our models. For instance if all we need is to estimate the rate of monomer consumption, and are not worried about deactivation by hydrogen, etc., then a simplified model in the form of Eq.(2) is appropriate in the case of homopolymerization [27][28].

$$R_p = k_p C^* C_{Et}^P \tag{2}$$

Where R_p is the rate of polymerization, k_p a lumped propagation rate constant, C^* is the concentration of active sites, C_{Et}^P is the concentration of ethylene at the active site. Even in this oversimplified form, one needs an accurate expression for the lumped parameter $k_p C^*$ that can empirically account for activation and deactivation of the catalyst that would need to be fit from experimental data. An equivalent simplified form for the copolymerization rate expressions could be used to calculate rate and average composition in the case of copolymerization (*e.g.* [29]). In this case one would need 2 propagation rate constants and 2 reactivity ratios at the very least.

If the estimation of average molecular properties, such as number- and weight-average molecular weights is needed, then it is necessary to solve the entire set of equations shown in Table 2 using, for example, the method of moments. If one is considering an ideal, single-site catalyst, then set of equations shown in Table 2 is sufficient. However, in this case it is necessary to know as many as 17 rate constants, two reactivity ratios and the concentration of

active sites for a single site catalyst. On, the other hand, if we wish to model the molecular weight distribution for a CrO_x, or Ziegler-Natta catalyst, then we also need to know the number and relative fractions of families of active sites that are representative of the catalyst in question (impossible to know *a priori*), and whether or not these quantities change during the polymerization [30]–[34]. Difficulties with determining these values have been discussed elsewhere [1]. In particular, estimating the active site concentration or fraction of active metal centers is also a very challenging task. Practically the only thing we can say about this quantity is that the number of active centers is less than the number of transition metal molecules in the catalyst [35]–[37]. For further discussion of modelling microscale kinetics, the reader is directed to references [1], [18], [19], [25], [27], [38].

It is also important to repeat that even if one has a good microscale model, it is absolutely necessary to know the temperature and concentrations of the different species involved in the polymerization *at the active site*. If one is modelling a solution polymerization system, the conditions at an active site will be whatever they happen to be in the reactor at the point where the active site is found. On the other hand, in this paper we are interested in models for ethylene polymerization in the gas phase using supported catalysts: it is therefore necessary to impose a mesoscale model between the micro- and macroscales.

2.2   Mesoscale Modeling

We have (somewhat arbitrarily) defined the mesoscale as the length scale of the particles in the reactor. The reason for this choice is simple: as soon as active sites are deposited on (or in) a solid support, temperature and concentration gradients will form inside the particles if polymerization occurs. As knowledge of the temperature and concentrations of reactive species at the active sites is essential for the microscale model, it is obviously important to be able to predict these quantities at every point in the particle. Large gradients in the polymerizing particles will lead to wide changes in local rates of polymerization, molecular weights and copolymer composition; on the contrary, negligible gradients to a more homogeneous product. Modelling of these gradients relies on transport models combined with a microscale kinetic model. Writing transport models (*e.g.* the classical diffusion equation with chemical reaction) requires some representation of the particle morphology. In other words, in order to write the transport equations (heat and mass balances) one needs to understand (and in an ideal world, to predict changes in) the structure of the particles. Such models are often referred to as *Single Particle Models* (SPM).

For a number of reasons discussed at length elsewhere [22], [24], [27], , [39]–[45], [46], developing SPM can be a challenging task. As has been demonstrated many times, catalysts supported on silica or on $MgCl_2$ have at least 2 levels of organization. The simplest way to describe this is to say that the catalyst particles are in fact an assembly of smaller sub-particles. In other words, we can think of the catalyst particle as being a big spherical cluster (macrograin) that is made up of an assembly of smaller spheres (micrograins) that are physically attached to each other. After the catalyst is injected into the reactor, monomer(s), hydrogen and other compounds begin to diffuse toward the particles, through the external boundary layer and into the pores. The rate of diffusion through the pores during the initial instants depends on the pore structure of course, but also on whether or not the catalyst is injected dry, or, as is more likely, suspended in a hydrocarbon that fills the pores and slows down diffusion. As soon as the monomer reaches the surface of the micrograins in the pores where the active sites are found, it polymerizes. Monomer continues to diffuse into the pores, but now must dissolve in the polymer covering the active sites and diffuse toward the latter. Polymerization continues, and new polymer formed at the active sites pushes the older polymer away. Very rapidly stresses build up in the particles as polymer formed on one side of a micrograin or pore wall pushes against the polymer formed elsewhere. These stresses lead to the rupture of the physical bonds holding the micrograins together. This is referred to as *fragmentation*. This fragmentation process is rapid, but not instantaneous, and several papers show that it will most likely occur in pores that are most accessible to monomer, or, in the case of highly homogenous support structures, in a layer-by-layer manner, starting on the outside of the particle and moving inward [47]–[49]. Once fragmentation is complete, the process continues, and the particle grows by expansion as the new polymer is formed at the active sites.

Modelling this process is not straightforward, but it is nevertheless possible to develop meaningful models of the particle growth process that help us to understand the relative importance of different phenomena if we allow ourselves to make several simplifying hypotheses. There are two main types of SPM found in the literature [22]:

- The Multigrain Model (MGM): the final polymer particle is made up of primary particles. Each primary particle is a result of polymer growth around a catalyst fragment. Mass transport through the pores (by diffusion) and through the polymer layer surrounding the individual catalyst fragments are modelled separately. It is usually assumed that the morphology (shape, number of micrograins, etc.) of the final

11

polymer particle resembles that of the initial catalyst particle, *i.e.* the identity of each micrograin is retained.

- The Polymer Flow Model (PFM): along with the internal particle porosity, growing polymer chains and catalyst fragments form a pseudo-homogenous matrix, in which the active sites are dispersed. Accordingly, all transport steps are described in terms of effective diffusion coefficients, somehow accounting for the heterophasic nature of the particle.

For further information on single particle studies, the reader is directed to the available reviews [1][22][39][42]. Of the two, the PFM is simpler to write and to solve as one single set of coupled partial differential equations (PDE). The morphological representation of the MGM is somehow unrealistic as its mathematical structure assumes that the morphology of the growing polymer particle remains identical to that of the catalyst; *i.e.* it is an assembly of concentric layers of identical micrograins. This schematization does not allow for even empirical variations of particle morphology, and can be far from the real structure when significant interpenetration among the microparticles is taking place (which is often the case shortly after the end of fragmentation). The PFM is not necessarily significantly more realistic, but is a bit more flexible (and simpler). In this model the particle is said to consist of one, "pseudo-homogeneous" phase made up of a mixture of polymer and pores, and the transfer phenomena occur in this phase.

Some of the work from the group of Kosek at the ICT in Prague has demonstrated nicely that the final morphology depends on a balance between the initial structure of the particles, the rate of polymerization, and the polymer properties during the expansion of the polymer particles [43]–[46]. In theory could be used as a robust SPM if one had all of this information. However, such complex models are very expensive in terms of computational time. One needs an accurate description of the initial particle morphology; this is probably different for each catalyst particle. Furthermore, it is almost impossible to measure rapidly the changing physical properties with current techniques. For these reasons, Alizadeh and McKenna [24] point out that most current SPM studies do not use such complex descriptions, but rather rely on the PFM.

In the PFM, the coupled heat and mass balances are written as follows. The radial profile of the concentration of a given monomer in the growing particle can be described by the well-known diffusion reaction equations:

$$\frac{\partial M_p}{\partial t} = D_{eff} \frac{1}{r^2} \frac{\partial}{\partial r}\left(r^2 \frac{\partial M_p}{\partial r}\right) - R_p \qquad (3)$$

Typical boundary conditions are: (3a)

$$\frac{\partial M_p}{\partial r}(r = 0, t) = 0$$

$$D_{eff} \frac{\partial M_p}{\partial r}(r = R_L(t)) = k(M_b - M_p) \qquad (3b)$$

Initial Condition: (3c)

$$M_p(r, t = 0) = M_{p,0}$$

Where M_p is the evolving concentration of monomer inside the pore space of the pseudo-homogeneous phase that makes up the particle, t is the polymerization time, r is the radial position in the particle, D_{eff} is the effective diffusion of monomer in the macroparticle (*i.e.* through the pseudo-phase composed of pores and polymer), and R_p is the polymerization rate. k is the mass transfer coefficient in the external boundary layer, M_b the bulk monomer concentration in the reactor, and $M_{p,0}$ is the initial concentration of monomer in the particle. Note that, the radius R_L of the particle is a function of time so one would need an additional expression to account for particle growth as a function of the rate of polymer production. Alternatively, Eq.(3) can be solved at constant value of R_L for a given time interval, after which the particle radius is adjusted to account for the polymer formation, the concentration profiles are adjusted and the integration is restarted.

The same approach can be used for the energy balances:

$$\rho_p C_p \frac{\partial T_p}{\partial t} = k_c \frac{1}{r^2} \frac{\partial}{\partial r}\left(r^2 \frac{\partial T_p}{\partial r}\right) - (\Delta H_p)R_p \qquad (4)$$

Boundary Conditions:

$$\frac{\partial T_p}{\partial r}(r = 0, t) = 0 \qquad (4a)$$

$$k_c \frac{\partial T_p}{\partial r}(r = R_L(t), t) = h(T_b - T_p) \qquad (4b)$$

Initial Condition:

$$T_p(r, t = 0) = T_{p,0} \qquad (4c)$$

where ρ_p is the particle density, C_p the heat capacity of the particle, T_p the local particle temperature, k_c the particle effective thermal conductivity and ΔH_p the heat of polymerization. h is the film convective heat transfer coefficient and T_b the bulk temperature. $T_{p,0}$ is the initial particle temperature. The volumetric rate of polymerization R_p is dependent

on the concentration of monomer at the active sites and the local temperature, which means that:

- we need a reliable kinetic (microscale) model for the mesoscale model to be accurate;
- R_p changes as a function of radial position inside the particle;
- appropriate values of diffusion coefficients are available, taking into consideration polymer properties, temperature and the composition of the mixture of penetrants;
- since the rate(s) of polymerization depend on the concentration of monomer at the active sites, an accurate solubility model capable of accounting for the cosolubility effect of mixtures of species is used [50] [51].

In the frame of PFM, the effective diffusion coefficient for a single species can be calculated with an expression such as the following [52][53][54]:

$$D_{eff} = \frac{\varepsilon}{\tau^2} D_{pore} + (1 - \varepsilon)(1 + 3\varepsilon)D_{pol} \tag{5}$$

Where ε is the porosity of the particle, τ the tortuosity of the pores, D_{pore} the pore diffusivity, and D_{pol} the diffusivity of the monomer in the polymer phase. Assuming one can get a reliable estimate of the diffusivity of the species of interest in the pore space, in order to estimate the overall diffusivity it is still necessary to:

- know (*a priori*) the porosity and tortuosity of the particle. These parameters can change with time, and in reality, can be impacted by the rate of polymerization, polymer properties, phase of the reaction, etc.;
- be able to predict the diffusivity of the species of interest in the polymer phase. This in turn requires an accurate model for how the composition of the fluid in the pore space influences the free volume of the polymer and thus the solubility and diffusivity of the different species through it [51].

In order to include the boundary conditions one also requires precise and reliable heat and mass transfer coefficients between the particle and the bulk phase (*h*, *k*) [22], [28], [55]–[57]. Although the mass transfer in the film barrier surrounding the particle can be negligible in the gas phase, the heat transfer resistance can be significant and not so easily dismissed [56]. Various correlations have been reported in the literature, and we will discuss this more below. However, at lower Reynolds number around spherical particles, the calculated values for the

boundary layer heat and mass transfer resistance can differ by several orders of magnitude depending on the correlation chosen [56]. Some authors [55], [58], [59] have used the Ranz-Marshall correlation for gas-phase catalytic polymerization, others have used more complex ones. McKenna *et al.* [60] validated the Ranz-Marshall correlation for particles in highly diluted systems (where the particles do not interact with each other), but showed that when two particles are close enough that the flow field around them is modified, this correlation is no longer valid and will overpredict the value of Nu, and thus of the heat transfer coefficient. Chang *et al.* [61] also showed that particle-particle collisions in FBR are very important in determining the heat transfer rate, as are the shape, size, and nature of the particles themselves. It is more than likely that heat transfer coefficients will need to lump together not just purely convective effects, but also need to account for particle-particle interactions via the bed density and other physical characteristics of the reactor powder. This suggests that a decent reactor model will necessarily need an accurate description of mesoscale mass transfer, and perhaps more importantly, heat transfer coefficients.

3   Macroscale modeling

A macroscale model of gas-phase olefin polymerization describes what happens at the reactor scale and allows us to understand the relationship between the operating conditions, raw material feeds, the reactor/process configuration, productivity and polymer properties.

Before discussing macroscale models directly, let us revisit how production of polyethylene occurs in an FBR. First of all, it should be noted that for reasons related to economy of scale all reactors for commercial gas scale processes are continuous, meaning the catalysts and fluid components are continuously fed to the reactor, and the product and unreacted fluids are continuously withdrawn. The catalyst particles are either fed directly to the reactor or can be prepolymerized. Prepolymerization refers to a process step where the catalyst is used to produce a small amount of polymer slowly and under controlled conditions to improve morphology and the heat transfer characteristics of the particles. Either way, upon entering the reactor the particles are suspended in a stream of gas (or gas and liquid droplets) composed of monomer(s), hydrogen, and inert compounds. As described above, the reactive species are transported to the active sites from the continuous phase of the reactor, and the particles grow by expansion as polymer accumulates in them. How the polymerizing particles are distributed within the reactor, and how they are exposed to local variations in temperature and

15

concentration will determine how phenomena at the meso- and microscales occur (in other words, what kind of polymer we are going to make, and at what rate).

In order to fluidize a phase of particulate solids it is necessary to pass a rapidly flowing gas stream through it. At low fluid velocities (*i.e.* less than the minimum fluidization velocity, u_{mf}), the vapor stream passes through the interstices between the particles without displacing them. This is in fact a packed bed. As the velocity increases, at the minimum fluidization velocity u_{mf} the bed begins to expand homogeneously, the drag force on the particles from the gas flow is equal to the weight of the particles and the densely packed particles behave like a fluid. If the gas velocity is increased beyond u_{mf}, bubbles can form in the bed, which can expand further because of the bubble hold-up even though the pressure drop across the bed does not change. Increasing the gas velocity significantly above the minimum fluidization condition can cause operation to change from bubbling to slugging, and even to fast fluidization. If there is a particle size distribution of the solid phase, regulating the gas velocity can be a challenge because a high velocity might be needed for large particles, whereas this velocity might change the flow regime and cause the smaller particles to be blown out the top of the bed [2], [62]–[64]. This latter problem is (mostly) eliminated by having a disengagement zone at the top of the bed, where the diameter of the reactor increases by a factor of 2 or more, thereby causing the velocity of the gas above the bed to drop by a factor of 4. This causes the smaller particles to fall back down into the main part of the bed. It is usually assumed and accepted that FBR for polyolefin production work under what is called bubbling mode, shown schematically in Figure 3 [65][66]. In this mode, small bubbles form at the bottom of the reactor near the distributor plate and grow as they approach the top of the emulsion. In bubbling mode the reactor is said to contain two or three phases if no liquid droplets are present: (1) a dense emulsion phase composed of solid particles flowing down countercurrent to a gas stream flowing up at u_{mf}; (2) a much lighter bubble phase that travels through the emulsion and that is composed essentially of gas in excess of that needed for minimum fluidization and little to no solids; and (3) a wake phase corresponding to the solid-rich gas phase raising with the bubbles [67].
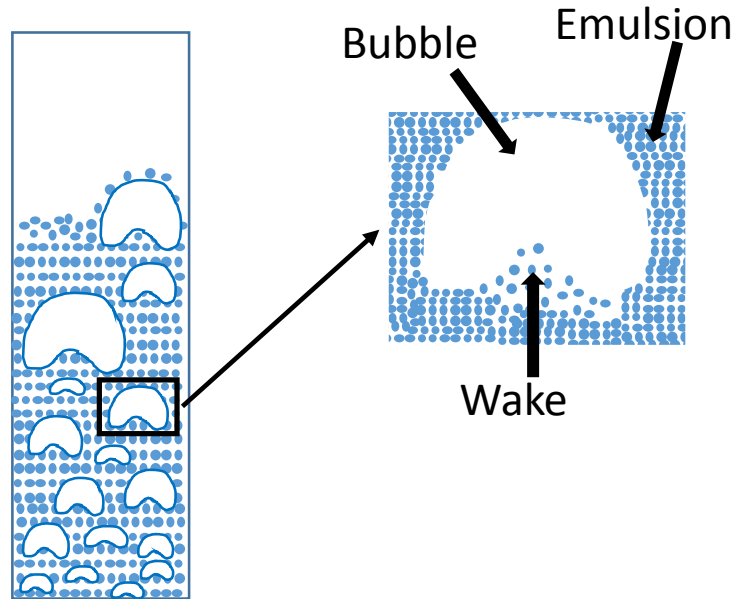
Figure 3. FBR operating in bubbling regime

In reality this schematization is quite rough since the emulsion phase can actually be less dense than at minimum fluidization. Moreover, as shown schematically in Figure 3, the bubbles are not spherical, rather the underside is thought to be somewhat convex, and in this region is found the *bubble wake* which drags a considerable amount of solids upwards. Turbulent mixing in the wake can help to promote heat and mass transfer between the emulsion and bubble phases [2].

Macroscale models of fluidized beds that do not employ CFD to describe the hydrodynamics of the reactor rely on different simplifying assumptions and representations of this bubbling mode. We will discuss each in more detail below. The models can be grouped in different ways, but we will classify them as single-phase (*i.e.* emulsion only) and multiple-phase models.

The simplest single-phase model describes the FBR as a perfectly mixed continuous stirred tank reactor (CSTR) that contains only an emulsion phase with a porosity equal to that at the minimum fluidization conditions. Even though the emulsion can exchange heat and mass with a uniform gas phase that is not actually modelled, it is not possible to include any form of axial (direction of gas flow) gradients with this approach. A refinement of the single phase CSTR model is to "break" the emulsion up into a certain number of compartments. In this representation, the reactor is essentially a cascade of CSTRs each one containing an emulsion

phase at minimum porosity. Each compartment can exchange energy and matter with the compartments immediately above and below it (except obviously for top and bottom compartments). This tantamount to including a minimal representation of the hydrodynamics. It allows us to account for temperature gradients in the emulsion phase, and if population balances are included, evaluate particle segregation.

More complex models will include two or more phases in order to account for the presence (and possibly composition) of the bubbles, bubble wake and even liquid droplets as a separate phase. In the multiple-phase models each emulsion compartment (we can have one, or more emulsion compartments) is a single, well-mixed zone. The bubbles can also be a single compartment (mixed or plug-flow type) or divided up into multiple-compartments that exchange heat and mass not just with neighboring bubble compartments, but also the emulsion compartments.

In addition to assumptions about the macroscale hydrodynamics, macroscale models must also include hypotheses about mesoscale phenomena. For instance, one could neglect intraparticle gradients, and assume that the concentrations at the active sites are in equilibrium with the composition of the external gas phase. Even though not generally applicable, this approach would allow one to capture changes in feed composition on productivity and average polymer properties in a reasonable manner. To include mesoscale phenomena in a more realistic way (thus obtaining a more reliable description of the process), it is necessary to integrate a single particle model into the reactor model. Intraparticle gradients can then be accounted for either by assuming that all particles have the same representative diameter, or by calling upon Population Balance Equations (PBE) that can account for the age, size, composition and molecular weight distributions of the particles. This will give us a much more detailed and realistic picture of the polymerization, but this picture will only be as accurate as all the additional model parameters and correlations needed to solve the model.

Since PBE can be used with both single- and multiple-phase models, let us rapidly discuss their use in the models of interest.

3.1   Population Balance Equations

Readers interested in an in-depth discussion of population balances in general are referred to the book of Ramkrishna [68], while the use of PBE in polymerization processes is discussed in detail *e.g.* by Kiparissides *et al.* [69]. In our specific case, we are often interested in

properties that can be influenced by the size of the catalyst/polymer particles. Heat and mass transfer resistances associated with polymerization in particulate systems will have an influence on the molecular weight and copolymer composition distributions, on the temperature (and thus stickiness or softness) of the particles themselves. Such resistances will increase as the catalyst particle size increases, as the porosity of the particle decreases, or as the intrinsic activity of the catalyst increases. As we are dealing with continuous reactors, the exit age or residence time distribution of the solid phase in the reactor means that particles can have different ages in the reactor(s) of one's process. This is coupled with the fact that the activity of most catalysts will be a function of time (they activate and/or deactivate during the polymerization). Thus, if we need information about the particle size distribution, we need to take into consideration all the different phenomena that can influence the PSD. This is often done using population balances.

The assumption behind the formulation of population balances is that for each point in particle state space there is an associated function describing how the population of particles with a given set of properties changes as a function of time (or spatial position, etc.). In practical terms in an FBR for the production of PE, the population balances have the following terms for particles in the size interval $[d, d + \Delta d]$ inside a given well-mixed zone:

$$
\begin{pmatrix} Accumulation\ of \\ particles\ of\ size \\ between\ d, d + \Delta d \end{pmatrix} \tag{6}
$$

$$
= \begin{pmatrix} particles\ that \\ grow\ by\ polymerization \\ to\ attain\ size\ rd, d + \Delta d \end{pmatrix} + \begin{pmatrix} particles\ flowing \\ into\ zone\ with\ size \\ between\ d, d + \Delta d \end{pmatrix}
$$

$$
- \begin{pmatrix} particles\ flowing \\ out\ of\ zone\ with\ size \\ between\ d, d + \Delta d \end{pmatrix} + \begin{pmatrix} particles\ created\ by \\ agglomeration\ with\ size \\ between\ d, d + \Delta d \end{pmatrix}
$$

$$
- \begin{pmatrix} particles\ that\ dissapear\ by \\ agglomeration\ to\ make\ size \\ larger\ than\ d, d + \Delta d \end{pmatrix} + \begin{pmatrix} particles\ created\ by \\ attrition\ with\ size \\ between\ d, d + \Delta d \end{pmatrix}
$$

$$
- \begin{pmatrix} particles\ between \\ d, d + \Delta d\ that\ disappear \\ due\ to\ attrition \end{pmatrix}
$$

While the meaning of the first three terms on the right-hand side is quite clear, the remaining terms deserve some explanation before moving to the reactor models.

Particle agglomeration is usually described as a two-body problem, assuming that when two particles collide with each other, agglomeration may occur with a certain probability and a single particle with volume equal to the summation of the volumes of the two colliding particles is formed. The corresponding agglomeration rate is defined as the number of particles formed by agglomeration between two particles per unit time and unit volume and it can be given as:

$$\mathcal{R}_{ag}(i,j) = K_{ag}(d_i, d_j)n_i n_j \tag{7}$$

Where R_{ag} is the rate of agglomeration of particles of diameters d_i and d_j, respectively, n_i and n_j indicate the number of particles of size i, j per unit volume of reactor and K_{ag} is referred to as the agglomeration kernel. There is very little experimental and theoretical evidence regarding particle agglomeration for the case of gas-phase production of polyolefins. For this reason, an empirical approach is almost invariably used. In general, it is accepted that the agglomeration kernel will depend on the size of both colliding particles, temperature, polymer adhesive properties and polymer softening temperature [70] [71]. There is no clear-cut consensus on how to define the agglomeration kernel for two particles of diameters d_1 and d_2, but most modelling efforts usually follow a structure like the one presented by Arastoopour, Huanh and Weil [72]:

$$K_{ag}(d_1, d_2) = K_0(d_1^4 + d_2^4)(d_1^{-3} + d_2^{-3}) \tag{8}$$

Where K_0 is an agglomeration rate constant, given by:

$$K_0 = k_1 \exp\left[k_2(T_{s,1} + T_{s,2})/T_{sf}\right] \tag{9}$$

Here, k_1 and k_2 are proportionality constants, $T_{s,1}$ and $T_{s,2}$ are the particle surface temperatures and T_{sf} is the average polymer softening temperature. Eq. (8) shows that the formation of agglomerates will increase exponentially with increased temperature and especially when the particle surface temperature reaches the particle softening temperature. There are many factors that can impact the softening temperature, such as co-polymer composition of the polymer, polymer density or presence of an ICA [70][73][8]. In addition, one might ask if the softening temperature is in fact the best indication of stickiness, and several patents discussed in McKenna [5] cite the melt initiation, or melt onset temperature, as the most important indication of stickiness. Like the softening temperature, this value will also be a function of polymer density, degree of swelling and eventually molecular weight

distribution (MWD). Again, like the softening temperature, theoretical expressions are not available to help us predict its value for a given situation.

The impact of agglomeration has been discussed by Yiannoulakis *et al.* [74]. They considered the FBR to be well-mixed with the residence time distribution of an ideal CSTR, PFM as single particle model and a PBE of the form shown above. The authors showed that smaller particles have a higher tendency to agglomerate, as their surface temperature is closer to the softening temperature. The authors also showed the effect of temperature on PSD. As the temperature increases, the peak in the PSD shifts towards bigger sized particles, while the corresponding shape broadens. The long tail at the end of the curves at higher temperatures is caused by agglomeration. Dompazis *et al.* [70] extended the work done by Yiannoulakis and coworkers [74]. A detailed simulation was carried out to study the effects of particle agglomeration on the end-use properties of the agglomerated polymer particles. It was found that the agglomerated particles will generally exhibit lower values for MW due to longer diffusion length scales and higher concentration gradients inside the particles. Although there is still very little progress in the experimental field that would allow for better correlations, the work by Dompazis and co-workers [70] represents a good starting point.

Furthermore, other agglomeration processes are important, including deposition on reactor walls due to static electricity (not to mention the increasing bed voidage due to repulsion between electrically charged particles [75], [76]), and due to liquid bridging in condensed mode. Finally, as mentioned above, only 2 body collisions are considered in agglomeration studies. There are several different explanations for why one does not consider 3 or more particle collisions in an agglomeration process. Most likely, the probability of a 3-body collision happening is much lower than that of a 2-body collision. Furthermore, the shape of the agglomerates is open for discussion. In the case of polyolefins, the result is a particle agglomerate that can have a different shape, and thus a different fluidization behavior than that of the original "spherical" particles [71]. To the best of our knowledge, there are no agglomeration kernels that allow us to take these important mechanisms into consideration in the coagulation kernel. So, while population balances are very useful tools, they should be approached with caution if we need to account for particle agglomeration in the process of interest.

Particle attrition, or fines generation, is a real and significant problem in FBRs for polyolefin production, as it can simultaneously increase the number of particles and reduce particle size,

which may affect reactor performance, fluidizing properties, operating stability and operating costs. Significant work has been done to study attrition in a range of non-polyolefin applications [77], but despite its undeniable importance in many olefin polymerizations, very little is known about how to include attrition in population balances for the system of interest here.

It is known that hard polymer particles are correlated with fines generation due to attrition, or particle breakage [78]. Presumably, they are more brittle, and thus break more easily than softer, more elastic particles. Some patents describe certain actions that help reduce fines generation (presumably through attrition) including raising the reactor temperature to soften hard, dense particles [79][80], or adding induced condensing agents for the same reason [12]. It is also very likely that the evolution of particle morphology in the FBR will influence attrition. For instance, if the particle fragmentation and expansion steps mentioned above lead to flakey or irregular particles, it is far more likely that these particles break than if the morphology is rounder and more compact. An example of this is seen in Figure 4. To avoid this, some patents also claim that attrition can be removed by reinforcing the structure of the catalyst support [81][82].
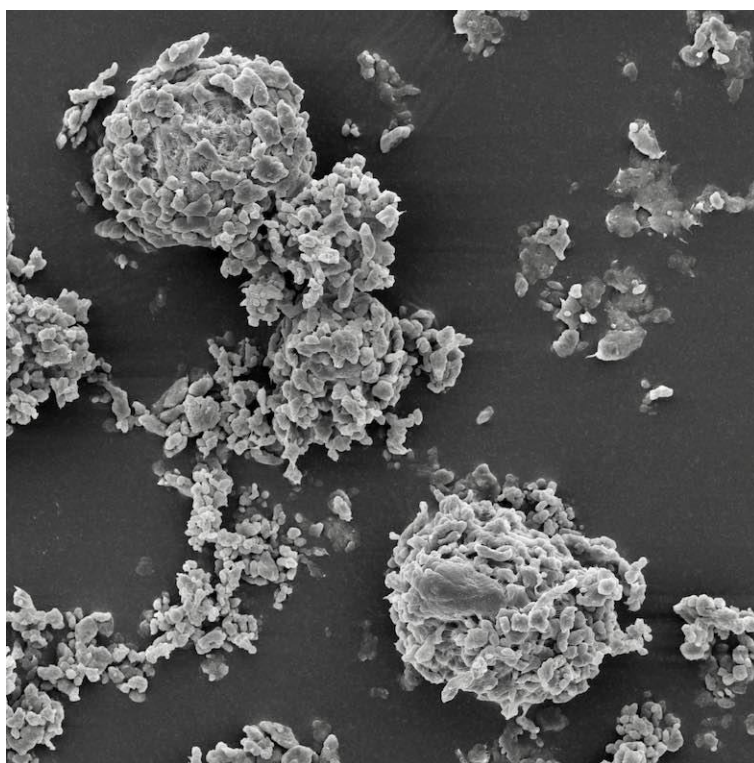

Figure 4. Example of particles amenable to attrition produced in gas phase polymerization of ethylene at 12 bars of ethylene, 80°C with a Ziegler-Natta catalysts.

Given the inherent complexity in modelling attrition, it appears that the few authors who tried to account for this simply used an oversimplified attrition rate with first order with respect to the particle number and constant, size-independent rate coefficient [71][83]. About the impact of attrition, Hatzantonis *et al.* [71] considered that attrition can significantly narrow the PSD in the bed and increase the amount of fines in the elutriation stream. As the attrition rate constant increases the bed PSD becomes narrower and its peak position shifts to smaller sizes. Furthermore, the smaller particles can be preferentially situated in the upper regions of the bed.

This very short discussion shows that the development of a comprehensive PBE relying not just on flow and particle growth, but that includes more complex phenomena that we know can occur is a real challenge. The validation of the proposed aggregation and attrition kernels by comparison with a large enough set of experimental data also in terms of PSD is still missing and would represent a major step forward when predicting the polymer PSD in this type of reactors.

3.2 One Phase Models

3.2.1 CSTR Approximation

The simplest way to model a fluidized bed reactor is to treat it as a continuous stirred tank reactor (CSTR) that contains a well-mixed emulsion phase that can exchange matter and energy with a uniform gas phase. Any impact of bubbles in the bed is neglected. McAuley and coworkers [84] were the first to propose this approach, and based their choices on the argument that the low per-pass conversion and back-mixing between the gas and solids ensures that any concentration gradient of monomer along the vertical axis is very small, and can therefore be neglected. Thus, the concentration of the monomer in gas-phase is constant throughout the reactor, while both the heat and mass transfer rates between gas and solid phases are sufficiently high to make acceptable a description of the reactor content as one single pseudo-homogeneous phase. The obvious advantage of this approach is the mathematical simplicity, which allows the researchers to focus on other issues.

Depending on the level of detail in the kinetic model employed, this model can be readily used for the prediction of production rate, monomer conversion, and polymer properties such as the MWD and the copolymer composition distribution (CCD). If a population balance is added, predictions of particle size distributions are also obtainable. Table 3 resumes some of

the studies in the literature that use a one-phase, well-mixed model approach. It is clear from this table that there is a vast array of applications of the one-phase models. For instance, Khang *et al.* [85] made use of a simple PBE and studied the effects of non-ideal mixing, by introducing a particle size-dependent RTD of the reactor and concluded that the assumption of perfect mixing for the solid is quite adequate for the PSD under typical operating conditions. Alves and co-workers [86] included a thermodynamic model, the Sanchez-Lacombe Equation of State (SL-EoS), to predict the effects of adding gaseous ICA to the reactor on production rate, reactor temperature and polymer PSD.

However simple models like this fail to capture the mass and heat transfer behaviors that happen between the bubbling gas and emulsion phases, which forcibly leads to an incomplete description of the reactor. Thus, simple one phase single CSTR models can be fitted to experimental data and used for specific case studies, although this diminishes the autonomy of the model predictions and the range of simulation results that can be obtained. An interesting overview of some of these applications can be found in reference [15], where it can be seen that these well-mixed models are used to predict and/or control overall quantities such as the production rate, outlet temperature, polymer density and melt flow index (MFI), monomer concentrations/pressures, and the bed height.

Ref	Polymerization	Dynamic/ Steady State	Energy Balance	PSD	MWD	CCD	MFI	Thermodynamic Model	Grade Transition	Validation With Experimental Data
[3]	Co-polymerization ethylene-1-butene	Dynamic	Yes	No	Yes	No	Yes	No	No	Yes
[84]	Co-polymerization ethylene-1-butene	Dynamic	Yes	No	Yes	Yes	Yes	No	No	Yes
[87]	Co-polymerization ethylene-1-butene	Dynamic	Yes	No	Yes	No	Yes	No	Yes	No
[88]	Co-polymerization ethylene-1-butene	Steady State	No	Yes	No	No	No	No	No	No
[85]	Homopolymerization	Steady State	No	Yes	No	No	No	No	No	No
[89]	Co-polymerization ethylene-1-butene	Dynamic	Yes	No	Yes	No	Yes	No	Yes	No
[90]	Co-polymerization ethylene-1-butene	Dynamic	Yes	No	No	No	Yes	No	Yes	Yes
[91]	Co-polymerization ethylene-1-butene	Dynamic	Yes	No	Yes	Yes	No	Yes	No	No
[92]	Co-polymerization ethylene-1-butene	Steady State	Yes	No	Yes	No	Yes	No	No	Yes
[86]	Homopolymerization	Steady State	Yes	Yes	No	No	No	Yes	No	Yes

Table 3. Overview of one-phase, well mixed models.

3.2.2 Compartmentalized Emulsion Models

Recall that in an FBR the particles are suspended by a flux of gas made-up of monomer(s), hydrogen, and inerts. The particles entering the reactor typically have an average diameter on the order of 100 microns or less, but of course with a particle size distribution. These particles will grow as the polymerization proceeds but as the residence time distribution (RTD) approaches that of a CSTR, particles will stay for different times as well. All of this means that in a typical FBR particle sizes can range from 10 to 10^3 microns. Considering that the minimum fluidization velocity of a given particle, as well as its terminal velocity, are dependent on its size (diameter), an important question emerges: is the assumption of well-mixed emulsion phase valid if we need to go beyond estimating cumulative properties? What should we do if we need information about the possible relationship between the reactor operating parameters and particle segregation in the bed? Furthermore, since the polymerization is highly exothermic, and heat removal is a major concern, the fluids are typically fed to the reactor at a temperature several tens of degrees below the reactor outlet temperature. This can lead to important axial temperature gradients in the reactor in certain cases. For these reasons, the well-mixed reactor hypothesis, although useful in certain limiting cases, is limited in terms of its ability to capture details of the reactor performance.

To overcome these limitations and answer the questions cited above, it is possible to use *compartment models*. In the simplest form of a compartmentalized model, we can continue to neglect changes in the gas phase and divide the emulsion phase of the previous paragraph into a certain number of compartments as shown in Figure 5. In such a model, each compartment acts like a CSTR that can exchange particles with the neighboring compartments. This allows one to not only discriminate the PSD at different reactor heights, but also to estimate temperature gradients as a function of the bed height. One can include elutriation (the arrow leaving the top compartment in Figure 5) as well if particles that are over-fluidized in the top compartment are expected. On one side, more detail about how the particles circulate in the reactor means that we can obtain a better estimate of how the feed conditions, composition, gas velocities, etc. influence the reactor output. On the other side, it is important to underline here that obtaining an accurate picture from such models entails an appropriate choice of compartmentalization, along with accurate mass transfer coefficients for transfer between compartments and phases.
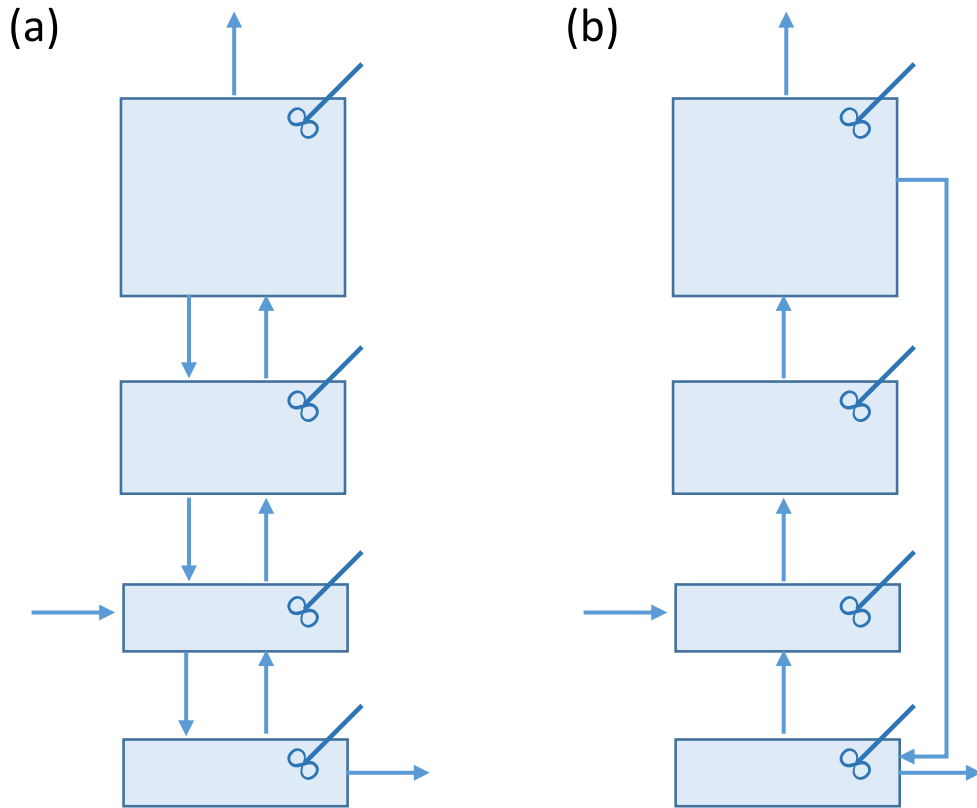
Figure 5. Compartmentalized emulsion model schema. (a) exchange of solids upward and downward between neighbouring compartments, and (b) all non-elutriated particles recycled to the bottom compartment. Arrows represent solid flows. Gas streams not shown as only the emulsion is modelled. Position of solid feed and product withdraw are arbitrary.

About the approach to compartmentalization, many variants have been proposed. As an example, in Figure 5(a) the solid is flowing upward and downward between neighboring compartments in order to somehow account for the solid exchange between gas and emulsion phase. On the other hand, in Figure 5(b) the particles can move upward through neighboring compartments, but not downward. In order to close the mass balance, the particles leaving the top compartment are "recycled" and fed into the bottom one [93]. This is a simplified approach which can result effective at specific conditions.

In most of the compartmentalized models, one can introduce population balances similar to those shown before, as well as the appropriate energy and mass balances. Perhaps the most difficult

part of the model is to adjust the flow rates of mass and energy between adjoining compartments in a reasonable way.

Ashrafi *et al.* [83] used a version of the simple compartmentalized model that does not explicitly contain a bubble phase, but allows for 2-way transfer of the emulsion phase between neighboring compartments to study the bed segregation in an FBR at low superficial velocity (Figure 5(a)). Based on a previous paper by Jafari *et al.* [94], the authors worked under the assumptions that their industrial scale reactor is divided into four CSTR's. The reactor model includes a PBE that accounts for particle agglomeration [72], constant rates of attrition using the model of Hatzantonis *et al.* [71] and elutriation. Their model showed that at a relatively low gas velocity (u_g = 0.25 m/s) the mean size of the particles decreases when moving up in the reactor. Bigger (and therefore heavier) particles are more difficult to fluidize, which explains their tendency to populate the bottom of the reactor. Dompazis *et al.* [93] used a compartmentalized emulsion model with a recycle stream (Figure 5(b)). Although the authors do not show the results in terms of superficial velocity, one can reason that the rate of recirculating solids is a measure of this parameter. The authors show that as the recirculation of solids is increased, *i.e.*, increasing superficial velocity, compartmentalized model collapses into the single CSTR model.

Alizadeh *et al.* [95] employed a compartmentalized emulsion model which was simply a "tanks in series" structure. While not explicitly stated, it appears that, like in the work of Ashrafi *et al.* [83], the reactor contained 4 equally sized compartments. Each compartment was considered to contain emulsion phase and bubbles that could contain solid particles [96], although how this model was applied for polyethylene is not explicitly stated either. In the conclusions, the authors actually said they neglected transfer resistance between the bubble and solid phases, so a pseudo-homogeneous state was assumed throughout the fluidized bed. They also suppose that the reactor was isothermal, that there are no intraparticle resistances, and that the particles can all be characterized by a single average size. They used a kinetic model from the literature to predict the properties of the produced polymer such as average molecular weight, polydispersity index and molecular weight distribution of polymer, and showed that the MFI predicted by the model was in decent agreement with actual plant data.

Table 4 summarizes a selection of available studies for compartmentalized emulsion models.

Table 4. Overview of compartmentalized emulsion models

Ref	Dynamic/ SS	Agglomeration	Attrition	Elutriation	MWD	MFI	Validation W/ Experimental Data
[83]	Steady State	Yes	Yes	Yes	No	No	Yes
[93]	Steady State	Yes	No	No	No	No	No
[95]	Steady State	NA	NA	NA	Yes	Yes	Yes

To summarize, the one-phase models are very attractive because of their simplicity. As with the CSTR approximation, this modelling approach can be definitely suitable to fit specific plant data. Nevertheless, this approach also comes with limitations. Considering the emulsion as a single phase, the description of the heat transport between the two phases is precluded and any temperature gradients in the reactor are ignored. Furthermore, Ashrafi *et al.* [83] fixed their model to 4 CSTR's and derived the PBE's to each compartment in a non-generic form, which means their equations cannot be applied to other reactor configurations/set-ups. More detail and flexibility require more complex process descriptions.

3.3   Multi-phase models

In reality, a FBR does not contain only an emulsion phase. It is widely accepted that FBR used for olefin polymerization operate in bubbling mode since the relative gas-particle velocities are much higher than the minimum fluidization velocity. This means an FBR can be thought of as containing 2 or more phases. If the FBR is operating in "dry" or "super dry" mode (*i.e.* no liquid in the reactor feed), we can identify separate emulsion and bubble phases, and eventually a wake phase, as sketched in Figure 3. However, if the FBR is operating in condensed mode, one also needs to include a liquid phase (the droplets) in at least part of the reactor.

Two-phase models can also be classified according to how the emulsion and bubble phases are treated: we can find models with the emulsion phase treated as a well-mixed CSTR that exchanges heat and matter with either a bubble phase (constant bubble size) or with a cascade of

bubble compartments (variable bubble size) the bubble phase can be treated as well mixed CSTR as or plug-flow, depending on the modeling approach. Finally, we can find models with both the emulsion and the bubble phases divided into compartments. Roughly speaking, even though we have enough degrees of freedom to adapt the model schematization to describe well the fluid dynamic and transport behavior of both the phases (thus improving the model accuracy), this increase of reliability comes at the price of being able to identify many more model parameters of difficult evaluation!

3.3.1 Constant bubble size

In the models discussed in this section, it is usually assumed that the emulsion phase is at minimum fluidization conditions, although some authors assume that higher fluidized porosity can occur due to excess gas [97]–[100]. The polymer, catalyst, and co-catalyst are all in the emulsion phase along with the gas fraction that ensures minimum fluidization. The bubbles contain the excess gas, and often it is assumed that there are no catalyst or polymer particles in the bubble phase.
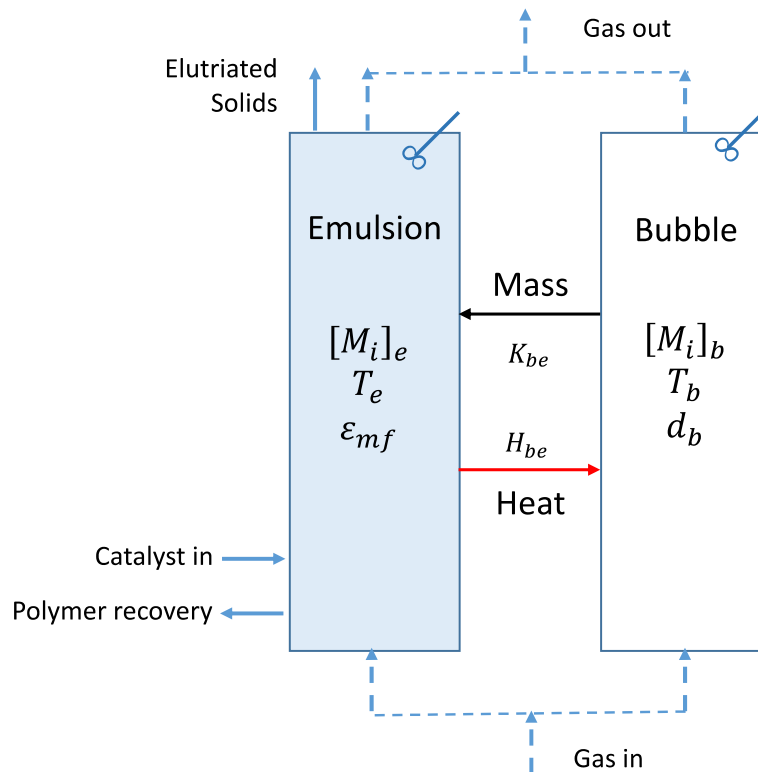
Figure 6. Two-phase constant bubble size model. Each compartment is treated as a CSTR. The symbols are defined in the text.

Choi and Ray [101] derived the first two-phase model applied to FBRs for olefin polymerization, based on the work of Kunii and Levenspiel [66]. Their model followed the assumptions discussed above, as well as the following ones: i) constant bubble size; ii) mass and heat transfer between the bubble and emulsion phases occurs at uniform rates throughout the bed; iii) negligible heat and mass transfer between the solid and gas in the emulsion phase; iv) negligible intraparticle heat and mass gradients. According to these assumptions, the mass balances for monomer i are derived for the emulsion and bubble phases:

Emulsion phase:

$$(\varepsilon_e V_e)\frac{d[M_i]_e}{dt} = U_e A_e\big([M_i]_{e,in} - [M_i]_e\big) - F_{recov}\varepsilon_e[M_i]_e - (1 - \varepsilon_e) R_{M_i} \tag{10}$$

$$+ K_{be}([M_i]_b - [M_i]_e)V_e\left(\frac{\delta}{1 - \delta}\right)$$

Bubble phase:

$$V_b\frac{d[M_i]_b}{dt} = U_b A_b\big([M_i]_{b,in} - [M_i]_b\big) - K_{be}([M_i]_b - [M_i]_e)V_b \tag{11}$$

In the above equations, the subscripts e and b represent the emulsion and bubble phase, respectively, ε represents the void fraction, V the volume of the phase, $[M_i]$ is the concentration of monomer, U is the phase velocity, A is the superficial area, F_{recov} is the polymer recovery rate, K_{be} is the bubble to emulsion mass transfer coefficient and δ represents the bubble phase volume fraction in the bed.

The enthalpy balance can also be derived for both phases. For the emulsion phase:

$$\left(\bar{C}_{p,e}(\varepsilon_e V_e) + V_e(1 - \varepsilon_e)C_{p,pol}\right)\frac{dT_e}{dt} \tag{12}$$

$$= U_e A_e \,\bar{C}_{p,e}\left(T_{e,in} - T_{ref}\right) - U_e A_e \,\bar{C}_{p,e}\left(T_e - T_{ref}\right)$$

$$- F_{recov}\left(\bar{C}_{p,e}\varepsilon_e + (1 - \varepsilon_e)C_{p,pol}\right)\left(T_e - T_{ref}\right) + (1 - \varepsilon_{bed})\Delta H_r F_{pol}$$

$$- H_{be} V_e \left(\frac{\delta}{1 - \delta}\right)(T_e - T_b)$$

For the bubble phase:

$$\left(\bar{C}_{p,b} V_b\right)\frac{dT_b}{dt} = U_b A_b \,\bar{C}_{p,b}\left(T_{b,in} - T_{ref}\right) - U_b A_b \,\bar{C}_{p,b}\left(T_b - T_{ref}\right) + H_{be} V_e (T_e - T_b) \tag{13}$$

Where T is the temperature of the phase, H_{be} is the bubble to emulsion heat transfer coefficient, T_{ref} is the reference temperature, C_{p,M_i} is the heat capacity of monomer i, C is the total number of species, U is the superficial phase velocity and A is the cross sectional area. The subscript *in* represents heat entering the phase. The overall thermal capacities of the two phases are defined as $\bar{C}_{p,e} = \left(\sum_1^i [M_i]_e \, C_{p,M_i}\right)$ and $\bar{C}_{p,b} = \left(\sum_1^i [M_i]_b \, C_{p,M_i}\right)$.

In bubbling fluidized beds, bubbles exchange mass and heat with the emulsion phase. Kunii and Levenspiel [66] assumed that mass is transferred from the bubbles to the surrounding clouds and from the clouds to the emulsion phase. The heat is transferred from the emulsion phase to the cloud and then to the bubble, as the reaction is exothermic.

For mass transfer:

$$K_{be} = \left(\frac{1}{K_{bc}} + \frac{1}{K_{ce}}\right)^{-1} \tag{14}$$

For heat transfer:

$$H_{be} = \left(\frac{1}{H_{bc}} + \frac{1}{H_{ce}}\right)^{-1}$$

<div align="right">(15)</div>

Where the subscripts bc and ce identify the mass and heat transfer coefficients between bubble and cloud and cloud and emulsion, respectively. Now, the mass and heat transfer coefficients calculated with equations (13) and (14) have been developed under the following assumptions: i) the gas superficial velocity (based on empty reactor) is considered to be at least the double of the minimum fluidization velocity ($U_o > 2U_{mf}$); ii) the velocity of rising bubble is considered to be at least five times the minimum fluidization velocity ($U_b > 5U_{mf}$); iii) the emulsion remains at minimum fluidizing conditions and the bubbles are solid-free. To the best of our knowledge, no experimental or theoretical studies are available in the literature assessing applicability and reliance of these correlations to the specific case of FBR for PE production.

The correlations required to evaluate some of the quantities involved in the previous balances are shown in Table 5. Even though the most commonly used correlations for both the bubble and emulsion phases are presented, other references are provided to direct the reader to different correlations than those shown. All symbols have already been defined, with a few exceptions: Ar represents Archimedes number ($Ar = gd_p{}^3\rho_{gas}(\rho_{pol} - \rho_{gas})/\mu_{gas}{}^2$, where g is the gravitational acceleration, d_p is the particle diameter, ρ represents the density of the gas and polymer – subscripts gas and pol, respectively – and μ_{gas} is the gas viscosity, H and D represent the reactor height and diameter, ε_{mf} represents the bed voidage at minimum fluidization conditions and k_g is the thermal conductivity of the gas.

Table 5. Correlations for two-phase model parameters. Adapted from [102][103].

Parameter	Formula	Ref	Alternative correlations
Minimum fluidization Reynolds Number	$Re_{mf} = (29.5^2 + 0.375Ar)^{0.5} - 29$	[104]	[2], [66]
Bubble velocity	$U_b = U_0 - U_{mf} + U_{br}$	[2]	[105], [106]
Bubble rise velocity	$U_{br} = 0.711(gd_b)^{0.5}$	[2]	[2], [105]
Emulsion velocity	$U_e = \dfrac{U_0 - U_b}{(1 - \delta)}$	[97]	[107]

Bubble diameter (constant bubble size)	$d_b = d_{bm} - d_{bm}(d_{bm} - d_{bo})exp\left(-\dfrac{0.3H}{2D}\right)$ $d_{bm} = 0.652\left[A(U_0 - U_{mf})\right]^{0.4}$ $d_{bo} = 0.00376(U_0 - U_{mf})^2$	[108]	[109], [110]
Bubble phase fraction	$\delta = 0.534\left[1 - \exp\left(\dfrac{U_0 - U_{mf}}{0.413}\right)\right]$	[96]	[2], [106]
Emulsion phase void fraction	$\varepsilon_e = \varepsilon_{mf} + 0.2 - 0.059\exp\left(\dfrac{U_0 - U_{mf}}{0.439}\right)$	[96]	[111]
Mass transfer coefficients	$K_{be} = \left(\dfrac{1}{K_{bc}} + \dfrac{1}{K_{ce}}\right)^{-1}$, with $K_{bc} = 4.5\left(\dfrac{U_e}{d_b}\right) + 5.85\left(\dfrac{D_g^{0.5}g^{0.25}}{d_b^{1.25}}\right)$ $K_{ce} = 6.77\left(\dfrac{D_g U_{br}\varepsilon_e}{d_b}\right)$	[2]	[66], [106], [112], [113]
Heat transfer coefficients	$H_{be} = \left(\dfrac{1}{H_{bc}} + \dfrac{1}{H_{ce}}\right)^{-1}$, with $H_{bc} = 4.5\left(\dfrac{U_e \rho_g \bar{C}_{p,b}}{d_b}\right)$ $\quad + 5.85\left(\dfrac{(\rho_g k_g \bar{C}_{p,b})^{0.5}g^{0.25}}{d_b^{1.25}}\right)$ $H_{ce} = 6.77(\rho_g \bar{C}_{p,b} k_g)^{0.5}\left(\dfrac{U_{br}\varepsilon_e}{3}\right)^{0.5}$	[2]	[66], [106], [112], [113]

When focusing on the condensed mode cooling, Mirzaei *et al.* [114] considered a steady state constant bubble size model where the reaction took place only in the emulsion phase and intraparticle resistances were neglected. While they considered liquid in the feed, they also assumed that it was immediately vaporized upon entry into the reactor so there is no need of a third phase, even though the energy balance includes an evaporative term. They also used the SL-EoS for the calculation of concentration at the active sites, but only considered pure component solubilities, so there are no co-solubility effects.

Zhou *et al.* [115] proposed an interesting variation on the two-phase model to study condensed mode reactors, which is illustrated in Figure 7. The authors say that the bubbles change size as they rise but assume that heat and mass transfer coefficients are a function of some average

bubble size (so for all intents and purposes this is a constant bubble size model). The emulsion phase is treated differently in order to accommodate the existence of an additional droplet phase of iso-pentane in the emulsion. The top of the emulsion phase is a well-mixed zone, but at the bottom the emulsion mixture and liquid droplets move upward in plug flow. The height of this gas-solid-liquid emulsion zone corresponds to the axial position where the last droplet evaporates. Using this model, they showed that allowing liquid in the reactor means that two very distinct zones can be seen, as per Figure 8. In the "wet" zone at the bottom of the bed (up to ≈ 1.5m in their conditions) the temperature rapidly increases as the droplets evaporate, creating a temperature gradient around 30 °C. The second zone extends to the rest of the bed with two phases (gas and solid) with a smaller temperature gradient of 7 °C They showed clearly that the temperature profile could have a noticeable effect on the molecular weight distribution if one neglects co-solubility effects. Zhou *et al.* validated their emulsion temperature profiles with industrial data (but did not give further information on the source of this data).
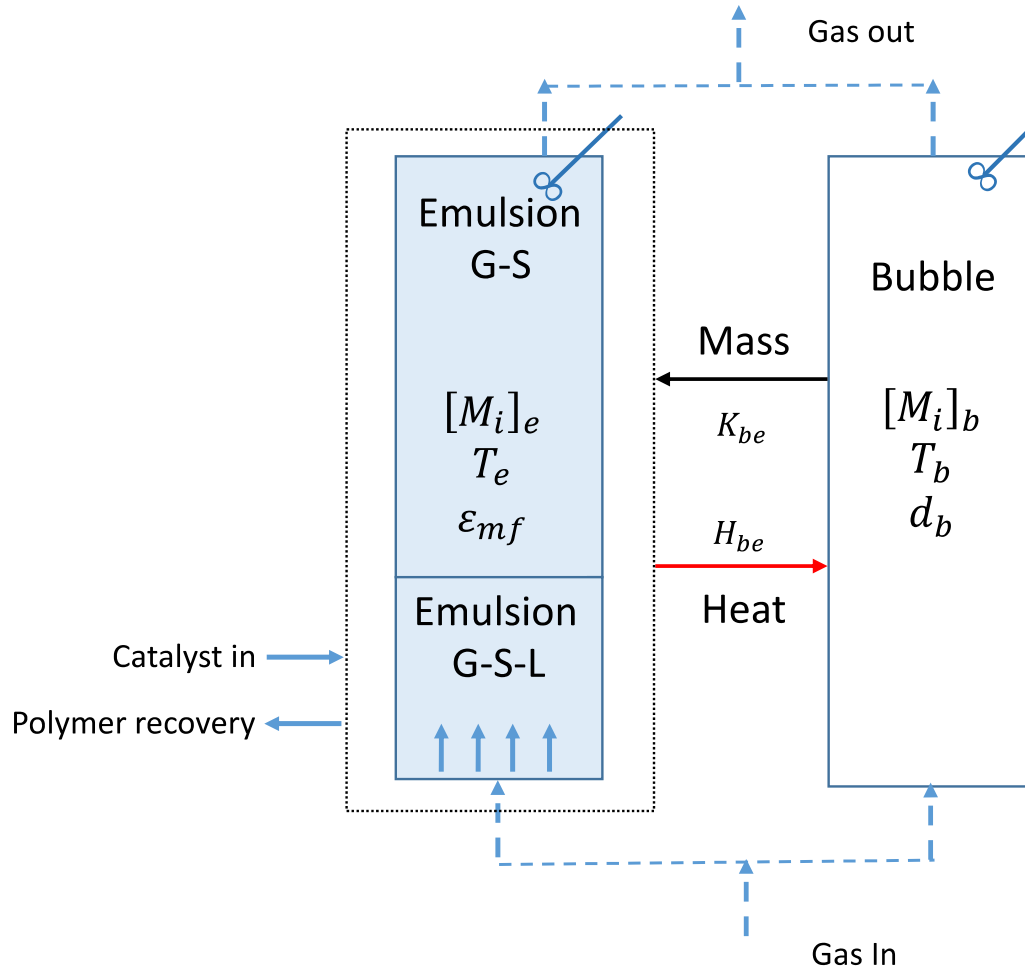
Figure 7. Two-phase model of Zhou *et al.* [115]. The emulsion phase is divided in a gas-solid-liquid (G-S-L) region at the bottom that moves from the distributor plate to the next zone via plug flow and in a gas-solid (G-S) upper region which is well-mixed. The bubble phase is a well-mixed zone.
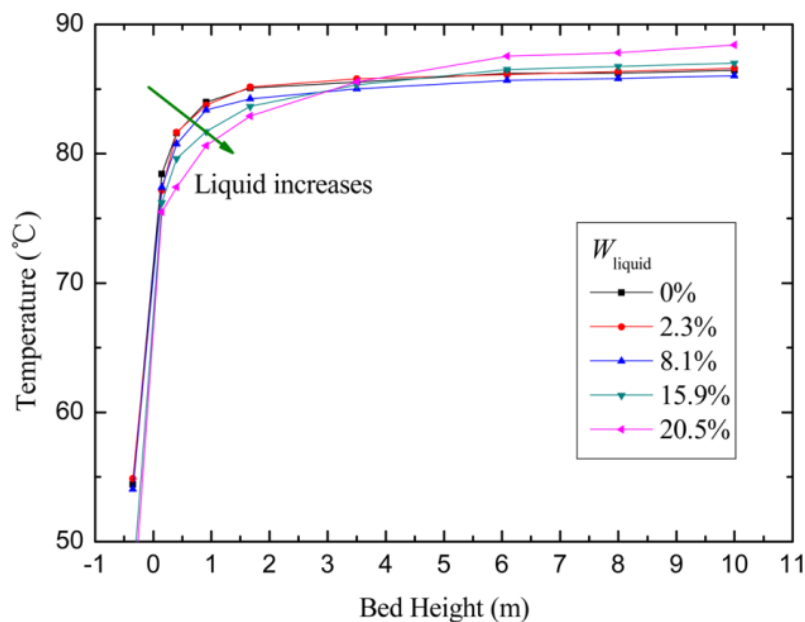
Figure 8. Axial bed temperature profiles. Reprinted with permission from Zhou *et al.* [115]. Copyright 2013 American Chemical Society

Fernandes and Lona [116] also considered a variant of the two-phase constant bubble size approach. Rather than treat each phase as well mixed, they modelled each compartment as a plug flow reactor, with the emulsion phase flowing downward and the bubble phase flowing up. They justified this by saying that as the particles grow, they will, on average, sink to the bottom of the reactor while the gas moves upwards, also in plug flow. For sake of convenience, the catalyst is injected at the top of the reactor and the polymer is recovered at the bottom, without solids recirculation. The reactor model consisted of mass and energy balances on the emulsion and bubble phase, and since each are treated as plug flow reactors, it was possible to calculate temperature gradients in the reactor. The authors coupled their model with a kinetic model to arrive at polymer properties profiles that vary with reactor height, such as average molecular weight, MFI and polydispersity.

These, and other constant bubble size modeling efforts that have not been discussed in here, are summarized in Table 6 for the reader's convenience.

Table 6. Overview of constant bubble size models.

Ref	Polymerization	Dynamic/ SS	Energy Balance	PBE	MWD	CCD	MFI	Thermodynamic Model	Validation W/ Experimental Data
[3]	Co-polymerization ethylene-1-butene	Dynamic	Yes	No	Yes	No	Yes	No	Yes
[101]	Ethylene and Propylene homopolymerization	Dynamic	Yes	No	No	No	No	No	No
[103]	Co-polymerization ethylene-1-butene	Dynamic	Yes	No	Yes	No	Yes	No	Yes
[114]	Co-polymerization ethylene-1-butene	Steady State	Yes	No	Yes	No	Yes	Yes	Yes
[115]	Ethylene polymerization	Steady State	Yes	No	Yes	No	No	No	Yes
[116]	Co-polymerization ethylene-1-butene	Steady State	Yes	No	Yes	Yes	Yes	No	No
[117]	Co-polymerization ethylene-1-butene	Steady State	Yes	No	Yes	No	No	No	No
[118]	Co-polymerization ethylene-1-butene	Dynamic	Yes	No	Yes	No	No	No	No
[119]	Co-polymerization ethylene-1-butene	Dynamic	Yes	No	Yes	No	Yes	No	Yes
[120]	Ethylene homopolymerization	Steady State	Yes	Yes	No	No	No	No	No
[121]	Ethylene homopolymerization	Dynamic	Yes	Yes	No	No	No	No	Yes

While the constant bubble size model might be a good exercise and an initial approach to reactor modelling, it is important to critically think about some of the approximations required for its implementation. When using this model, one faces an inherent dependence on empirical or semi-empirical correlations, as shown in Table 5. Those rely heavily on the bubble diameter that upon entering the reactor immediately reaches its maximum and stable size, which is of course an oversimplification of the actual bubbling fluidization. Another common approximation is to assume that the heat transfer resistance between particles and gas in the emulsion phase is negligible. The presence of a temperature gradient between particles and gas phase is well documented and can be quite important [28][55]. Furthermore, the only way to account for temperature gradients is once again to circumvent the well-mixed compartments either via a plug flow approximation, or a combination of plug flow and well-mixed zones.

3.3.2   Variable bubble size

The variable bubble size model is a natural and necessary extension of the constant bubble size model, since the bubbles grow by coagulation when they rise through the reactor, increasing in size with increased bed height. At the bottom of the bed, near the gas distributor, the bubble's size is at its minimum. This phenomenon was captured by Kunii and Levenspiel [2], [65], [66], but applied to the specific case of olefins polymerization by Hatzantonis *et al.* [102]. However, the idea of varying the bubble size had already been discussed by McAuley *et al.* [122] in an earlier study. In the variable bubble size model, the emulsion phase is still treated as a CSTR, but the bubble phase can be described with the use of compartments, set to have a height equal to bubble diameter, with the bubbles growing each compartment, as seen in Figure 9. The local heat and mass transfer between bubble and emulsion, local bubble volume fraction and rise velocity are now dependent on the size of the bubble and therefore on the corresponding bed height.
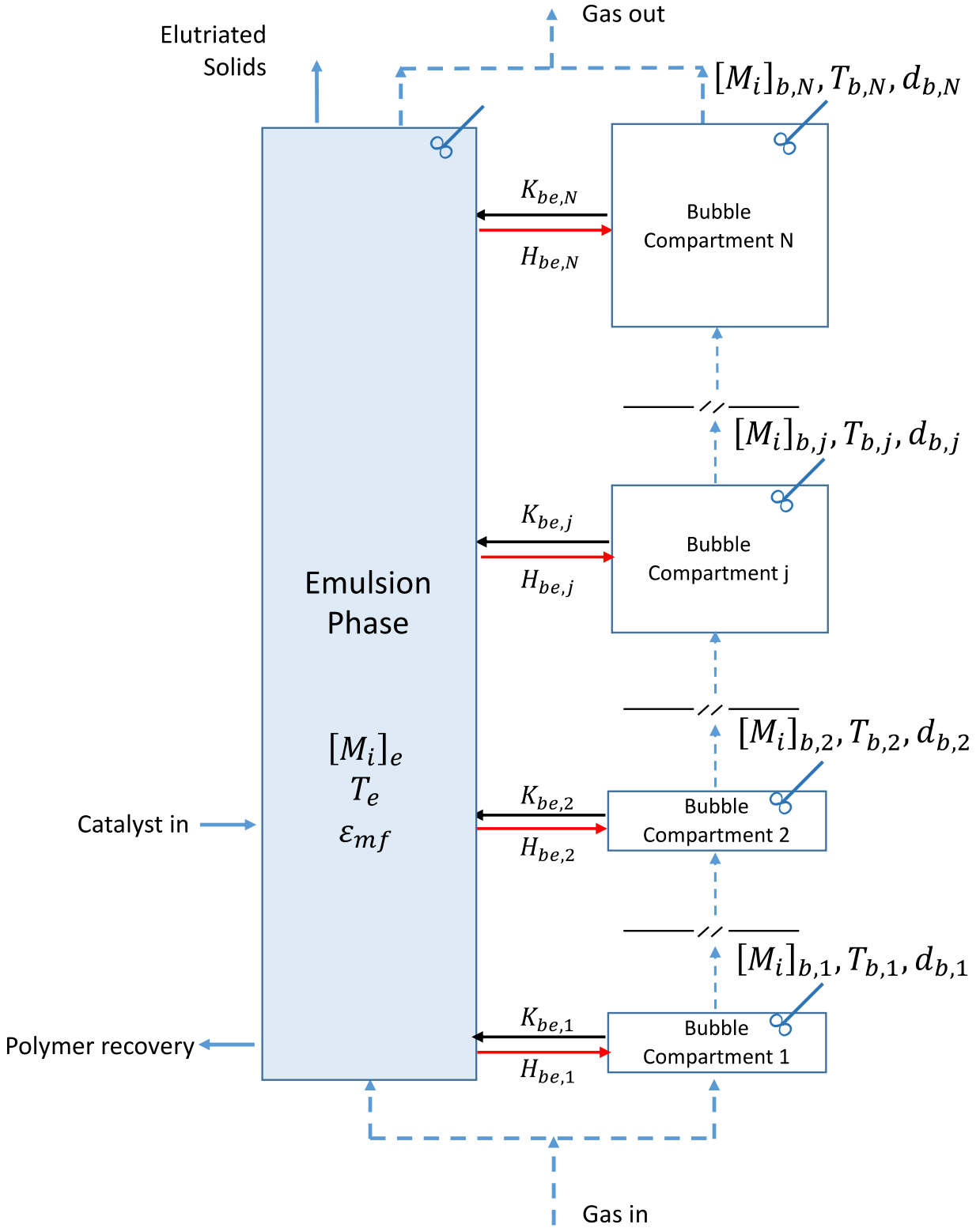
Figure 9. Schematic of the variable bubble size model. Adapted from [102].

The appropriate mass and enthalpy balances can be derived for this system. Here the emulsion phase balance remains the same as shown for the constant bubble size model, as no further assumptions have been lifted. For the bubble phase, the generic n-th compartment can be modelled as having a constant bubble size:

$$V_{b,n}\frac{d[M_i]_{b,n}}{dt} = U_{b,n}A_{b,n}([M_i]_{b,n-1} - [M_i]_{b,n}) - K_{be,n}([M_i]_{b,n} - [M_i]_e)V_{b,n} \tag{16}$$

The bubble volume, rise velocity and area are dependent on the bubble size, which means that the size of the bubbles needs to be calculated for each specific compartment.

The only additional information required for this model with respect to the constant bubble size model is the bubble diameter. Several correlations for this parameter have been developed over the years, so the particular equations shown in Table 7 are only to exemplify the type of information needed to include this level of detail in the models. Literature references to other correlations are also reported for the interested reader.

Table 7. Bubble diameter calculations for variable bubble size.

Parameter	Formula	Ref	Other correlations
Bubble diameter (growing bubble size)	$\frac{d_{b,max} - d_b}{d_{b,max} - d_{b,0}} = \exp\left(-\frac{0.3h}{D_{bed}}\right)$ where $d_{b,0} = 0.347[A(U_0 - U_{mf})/n_0]^{0.4}$ (Perforated plate) $d_{b,0} = 0.0037(U_0 - U_{mf})^2$ (Porous plate)	[108]	[2], [110], [123]–[126]

In fluidized beds, bubbles continuously grow until they reach a maximum bubble size, as a consequence of pressure drop and bubble coalescence. Above the maximum size, bubbles become unstable and can break up into smaller bubbles. Davidson and Harrison [106] assumed that the maximum bubble size is related to the particles terminal velocity (u_T):

$$d_{b,max} = 2u_T{}^2/g \tag{17}$$

However, most of the available correlations do not account for this maximum value. Therefore when using the variable bubble size model, a maximum bubble size should be used whenever a bubble size correlation predicts values larger than those obtained by equation (17)[102].

Hatzantonis *et al.* [102] investigated the effects of maximum bubble size. They found that imposing different maximum bubble sizes did not significantly affect the temperature and ethylene concentration predictions. Furthermore, they analyzed the impact of the maximum bubble size on the emulsion temperature for both variable and constant bubble size models. The variable bubble size model shows drastically less impact on emulsion temperature when compared to the constant bubble size model. This is thought to be a consequence of the improved bubble-phase mixing patterns, which results in more significant emulsion-to-bubble heat transfer rates. Furthermore, the mass transfer rate from bubbles to emulsion was shown not to affect the behavior of the reactor. Although this approach is still heavily reliant on correlations, the introductions of a variable bubble size has been shown to improve the model, as expected.

Comparing the well-mixed one-phase model and the models that account for either constant or variable bubble size is somewhat of a subjective exercise, as both methods deal with the same problem through different approaches. McAuley *et al.* [122] first compared the original two-phase constant bubble size model to their well-mixed one-phase approach. The authors compared the reaction temperature obtained from both models for various superficial gas-velocities and catalyst feed rates and showed that there was very little difference between the two. Also Hatzantonis *et al.* [102] compared the well-mixed one-phase model with constant and variable bubble size two-phase models without considering intraparticle heat and mass transfer resistances. The well-mixed and constant bubble size models were found to be limiting cases of the variable bubble size model. The reaction temperature was predicted to be highest with the constant bubble size, and lowest with the well-mixed model. Furthermore, they also found that the well-mixed and variable bubble size model yield similar results, different from those of the constant bubble size model.

In a similar vein, Ibrehem *et al.* [119] added a wake phase to the two-phase model (modified variable bubble size model), and compared simulation results using their model, the well-mixed, constant and variable bubble size models with plant data for emulsion temperature and MFI. The resulting three-phase model included heat and mass transfer resistances from the bubble to the wake, from the wake to the emulsion, and from the emulsion to the polymerizing particles. The authors assumed that the emulsion phase was at minimum fluidization conditions and they neglected intraparticle heat and mass transfer resistance. All 4 models predicted similar results in

the initial simulations. Using the adjusted model parameters, the authors were able to show good agreement with plant data (in terms of melt flow index and emulsion temperature). Once again, temperature gradients in the emulsion phase were ignored.

Even though this is not an exhaustive list of modelling studies, at this point one can conclude that there is very little difference in terms of model predictions between the well-mixed, constant and variable bubble size models in terms of productivity, emulsion temperature and basic polymer properties. Those differences that do exist appear to be mainly due to differences in the predicted emulsion temperature due to different heat transfer rates between the bubbles and the emulsion. Adding a further complexity in terms of a "cloud" around the bubbles and wake phase with solid entrainment does not seem to add any benefit in terms of understanding or predicting reactor performance. This should not be surprising given that when models treat the emulsion phase as well mixed this does not allow for temperature gradients along the reactor axis that might form under different conditions. At this point, if one wishes to estimate productivity and heat generation rates, and get an overview of how the process conditions impact the MWD and CCD based on a chosen set of kinetic and physical constants, there does not appear to be any significant benefit in adding the additional levels of complexity and finding the extra parameters and correlations required for the two-phase models. One can probably get a good overall picture of reactor performance from the well mixed model, which is in agreement with the conclusion from McAuley *et al.* [122].

As with the well-mixed model, these one- and two-phase models can be combined with PBEs to provide estimates of the whole PSD in addition to the quantities mentioned above. However, if one wishes to account for things like liquid in the reactor feed or allow for temperature gradients in the emulsion and/or gas phase, particle segregation by size, etc., then it is also necessary to complexify the models somewhat. This can be done using either fully compartmentalized representations of the reactor, or detailed hydrodynamic models based on CFD.

3.3.3   Fully Compartmentalized Models

At the risk of over-generalizing, the vast majority of modelling efforts of this type seems to employ the same approach, shown schematically in Figure 10. This model concept is based on the same fundamental assumptions that bubbles grow as they rise until they reach some

maximum size (*e.g.* Grace [127]) and that the emulsion phase is composed of communicating well mixed compartments. The gas compartments can be modelled either as a cascade of well-mixed zones of changing height (equal to the bubble diameter at a given height like with the previous model), or as being in plug flow (*i.e.,* a cascade of a large number of compartments, grouped as shown in Figure 10). Heat and mass transfer between bubble and emulsion phases are almost universally described using the transport coefficients developed by Kunii and Levenspiel [2]. Some works include solids in the bubble phase, some do not, and population balances can contain different terms from work to work. This seems to have a small impact on the bubble phase temperature gradients.

Most authors calculate a minimum fluidization velocity from an average particle size, which of course means that some small particles are over-fluidized (need to account for elutriation) and some are under-fluidized and can settle. Furthermore, given the challenge in validating the modelling work with plant data, only limited numbers of properties are compared for model validation. These observations do not mean that the modelling work is not of quality or is not useful; far from it. It means that the problem of modelling the FBRs for ethylene polymerization is attacked in very similar way, and employs a number of correlations that are not developed specifically for PE, or developed for uniform particle sizes, etc. Many of them can certainly give a decent estimate of the impact of changing one or more parameters on reactor behavior, and some can undoubtedly be fine-tuned to model specific processes. Obviously, producers do not make plant data available in the open literature, so the solution to the problem of model validation is certainly not readily available. A quick discussion of some fully compartmentalized models follows.
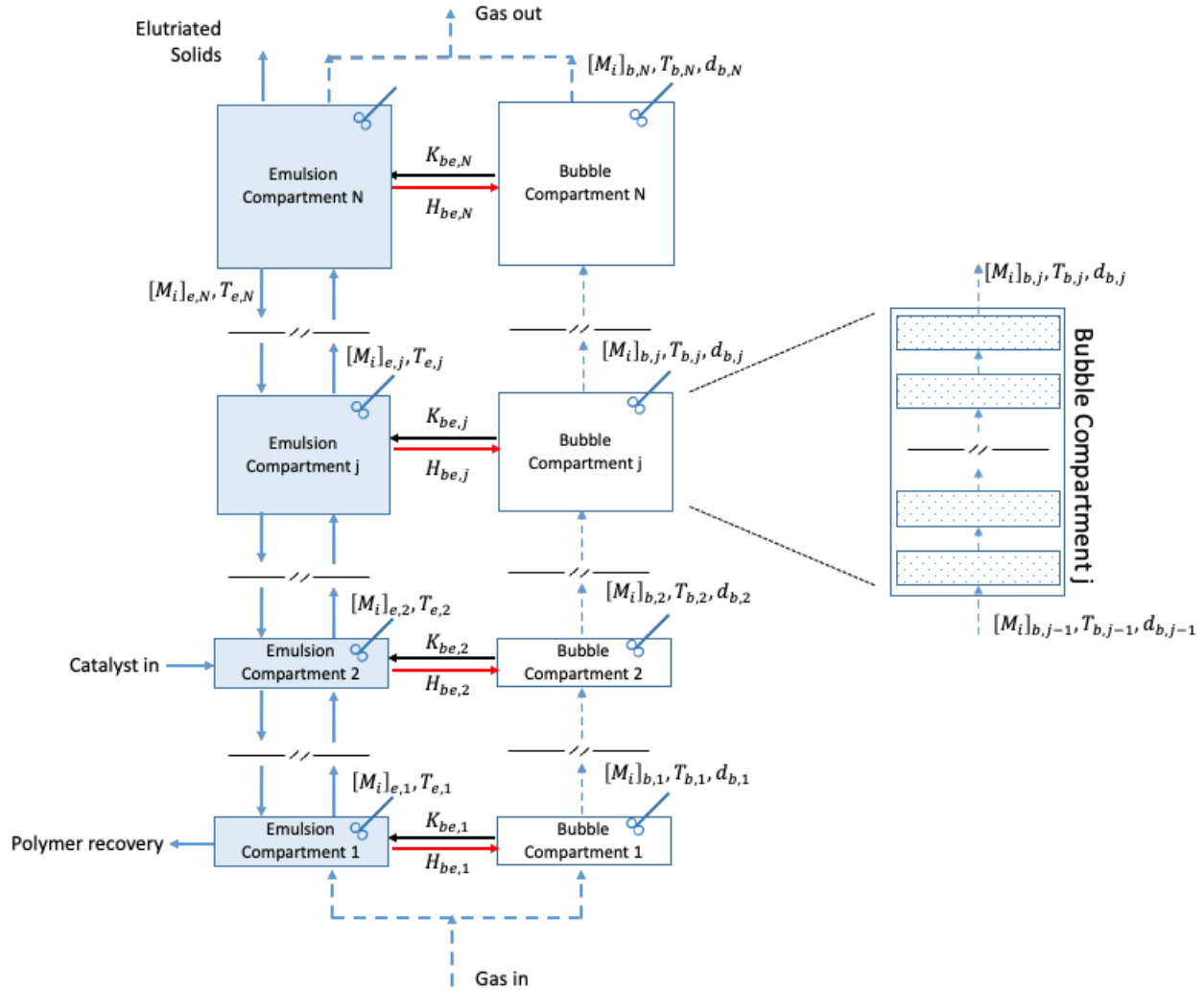
Figure 10. Concept of the fully compartmentalised model.

Following their earlier work, Ashrafi and coworkers [128] developed a two-phase model, which divided the reactor into compartments for both the emulsion and bubble phase and focused on the effects of operating conditions on bed segregation. As before, they used 4 CSTRs in series to describe the emulsion phase and added 4 PFR in series (same height as the emulsion compartments) to describe the rising bubble phase. The emulsion phase is described like in their earlier work [83], where the particles can either fall down to the compartment below or be blown up to the compartment above. The particles in the bubble phase are assumed to only move upwards, with the elutriated particles being recycled to the bottom compartment. They compared

the results of their isothermal simulations to plant data for the cumulative PSD and found reasonably good agreement (but it is not clear how the mass transfer rates between bubble and emulsion compartments were adjusted). While this model contains potentially more detail than their previous models, the overall predictions of PSD are quite similar. Without extensive comparison of a range of plant data it is not clear to us whether the addition of the bubble phase actually provides verifiable supplementary information with respect the simpler model presented early (especially since an energy balance is not included).

Kiashemshaki *et al.* [129] used a simple compartmentalized emulsion model with 4 compartments for each phase, and allowed a certain amount of particles to transfer between the phases. Here the fraction of particles in the bubble phase is calculated using a correlation that relates the superficial velocity with the minimum fluidization velocity. They used a 2-site kinetic model and assumed a uniform particle size. Simulated molecular weight distributions showed good agreement with plant data, and average bed temperatures were of a similar magnitude. It is not entirely clear what bed temperature this is, and no attempt is made to compare to plant temperature profiles. Furthermore, according to the simulations, about 20% of the total polymerization occurs in the bubble phase.

Dompazis and coworkers [130] developed a rigorous and complete multiscale, two-phase model, that included PBE (constant agglomeration, but no attrition). In this model the emulsion phase is in contact with a bubble and wake phase, and mass transfer from the emulsion to the wake portion of the bubble phase is accounted for. The authors focused on calculating the dynamic evolution of polymer properties (PSD and MWD) and the extent of particle segregation in the reactor. The authors claim that for higher superficial gas velocities, the PSD in both phases collapses to the same distributions, which is in agreement with the findings by Kim and Choi [131]. The emulsion temperature and single pass ethylene conversion decrease when internal mass transfer limitations are accounted for, due to lower polymerization rates. The authors saw the same trend for the PSD: the presence of internal mass transfer resistance led to smaller particles.

Farid and coworkers [132] also subscribed to the variable bubble size two-phase model, considering that the bed is divided into compartments and operates at uniform temperature. The authors also made use of populations balances to obtain the PSD inside the reactor. They saw that

increasing the number of compartments leads to bigger, but fewer bubbles. The authors also showed that the increasing the superficial velocity will decrease the bubble size.

Farag and co-workers [133] merged a two-phase variable bubble size model with a population balance model, while considering the reactor divided into compartments. They showed the effect of bubble size on the single pass conversion of ethylene, while varying the catalyst feed rate. Smaller bubbles have a lower velocity in the bed compared to larger bubbles. As a result, smaller bubbles lead to larger bubble number in the bed, and to a reduction in the volume of the emulsion phase. Therefore, the residence time of the solids decreases with a decrease in bubble size, reducing the contact time between ethylene and the catalyst. This is seen as a decrease in single pass ethylene conversion vs. bubble size. These results are in accordance with the findings of Dompazis *et al.* [130] on the same subject.

Table 8. Overview of fully compartmentalized models.

Ref	Polymerization	Dynamic/ SS	Energy Balance	PBE	MWD	CCD	MFI	Validation W/ Experimental Data
[130]	Co-polymerization ethylene-1-butene	Dynamic	Yes	Yes	Yes	No	No	No
[132]	Ethylene homopolymerization	Steady State	No	Yes	No	No	No	Yes
[133]	Ethylene homopolymerization	Steady State	No	Yes	No	No	No	Yes

An overview of these modelling studies is shown in Table 8. From these studies, it becomes clear that the addition of compartments to a model bridges the way to better reactor description, as it allows to axially discriminate the reactor while keeping the mathematical simplicity of well-mixed conditions for the emulsion phase. With this approach, it is possible to assess bed segregation, temperature profiles in the bed, or possibly extend these models for condensed mode case studies and infer on liquid hold-up. In return, these models come with several new parameters that need to be estimated, such as the flowrates of the streams that interconnect the different compartments, which might prove to be a challenging task depending on the overall compartments configuration. Still, even with a compartmentalized approach one is faced with an

enforced homogeneity in each "box", that can only be relieved with the use of computational fluid dynamics models.

4   Macroscale modelling with Computational Fluid Dynamics

Computational fluid dynamics simulations are becoming an established tool for the study of fluidized bed reactors and their increasing use is promoted by the combination of several factors. On the one side, they provide useful information about the gas and solid velocity fields inside the reactor, with a level of detail that is challenging to access experimentally as well as with the oversimplified description of fluid dynamics adopted with compartmentalized models. On the other side, CFD simulations are still computationally demanding but also more accessible by virtue of the increasing availability of high parallel computing (HPC) resources and the optimization of algorithms and numerical methods that aim at improving simulation efficiency.

Broadly, there are two main methods to deal with a fluid/solid multiphase system such as a fluidized bed reactor, according to the chosen approach for the description of the solid phase; in general, gas phase is taken into account as a continuum by means of continuity, momentum conservation and energy conservation equations, along with a suitable turbulence model.

In the framework of the Eulerian/Lagrangian (EL) approach, also referred as discrete particle model (DPM) or discrete element method (DEM), solid is modeled as a dispersed phase by explicitly including all particles in the system. Solid trajectories are computed by solving Newton's equation of motion for each particle, taking into account also particle-particle and particle-wall interactions. Although this approach is very detailed, since it allows tracking solid behavior at single particle level, its use is hindered by the prohibitive computational cost due to the large amount of particles usually present in a FBR reactor. EL is often the method of choice for the investigation of small labscale reactors characterized by low values of solid volume fraction (less than 10%).

Eulerian/Eulerian (EE) models describe the solid as a continuum, approximating the system as interpenetrating fluid phases. Analogously to gas phase, solid behavior is accounted for by means of continuity, momentum conservation equation and energy conservation equation, along with a

suitable turbulence model. Three main approaches can be employed in the framework of EE models [134]:

- Volume of Fluid (VOF) model: it allows tracking the temporal and spatial evolution of the interface between immiscible phases, by solving a momentum conservation equation for the interface and continuity equations for the volume fraction of the phases;
- Mixture model: it implies the solution of a single set of partial differential equations constituted by continuity, momentum and energy conservation equations for the mixture. Note that only relative velocities between phases can be obtained in this case;
- Eulerian model: continuity, momentum, and energy conservation equations are solved for each phase, whose coupling is performed by means of interphase exchange coefficients.

VOF and mixture models are not suitable for FBR reactors, because they do not provide a detailed description of the flow field of the solid phase, which can be achieved only by solving momentum conservation equations for each phase as done in the Eulerian model.

This motivates its extensive use for the FBR simulation: Eulerian model is more computationally expensive than VOF and mixture models but still constitutes a reasonable compromise between accuracy and computational efficiency, especially if compared with EL approaches. For the sake of completeness, a brief theoretical background of the Eulerian model is provided and discussed in the following.

4.1 Eulerian model: brief theoretical background

As mentioned, Eulerian model (EM) implies the solution, for each phase, of a system of partial differential equations composed of continuity equation and momentum and energy conservation equations, coupled with a turbulence model and appropriate correlations for the physical properties of the solid phase. The coupling between the phases is carried out by introducing appropriate interphase exchange coefficients. The presence of a polydisperse population of particles is accounted for through population balance equations (PBE) (vide infra). According to the EM implementation in CFD software packages like Ansys Fluent and OpenFoam, each considered particle size is modeled as a separate solid phase.

Conservation equations for gas and for each solid phase can be written as follows:

$$\frac{\partial \alpha_g \rho_g}{\partial t} + \nabla \cdot (\alpha_g \rho_g v_g) = -\dot{m}_{gs} \tag{18}$$

$$\frac{\partial \alpha_s \rho_s}{\partial t} + \nabla \cdot (\alpha_s \rho_s v_s) = \dot{m}_{gs} \tag{19}$$

where α, ρ and v are volume fraction, density and velocity, respectively, and the subscripts g and s indicate gas and solid phase, respectively. The term $\dot{m}_{gs}$ accounts for the interphase mass transfer from the gas to the solid, due to the diffusion of the monomer in the catalyst particles. Assuming that gas-solid interphase mass transport resistance and solid intraphase mass transport resistance are negligible, $\dot{m}_{gs}$ can be expressed as a function of the growth rate due to polymerization reaction.

If the gas phase contains more than one component, mass conservation equations are required as well:

$$\frac{\partial (\rho_g \alpha_g x_{g,i})}{\partial t} + \nabla \cdot (\rho_g \alpha_g x_{g,i} v_g) = -\nabla \cdot \alpha_g J_{g,i} + R_i \tag{20}$$

where $x_{g,i}$ is the mass fraction of component i in the gas phase, $J_{g,i}$ is the diffusive flux of component i in the gas phase and R_i is the net generation or production rate of component i, which can be due not only to chemical reaction in gas phase (if present) but also to interphase mass transport.

Momentum conservation equations for gas phase and each solid phase can be formulated in following form:

$$\frac{\partial \alpha_g \rho_g v_g}{\partial t} + \nabla \cdot (\alpha_g \rho_g v_g v_g) = -\alpha_g \nabla p + \nabla \cdot \overline{\overline{\tau_g}} + \alpha_g \rho_g g + \sum_{r=1}^{ns} K_{gr}(v_r - v_g) - \dot{m}_{gs} v_g \tag{21}$$

$$\frac{\partial \alpha_s \rho_s v_s}{\partial t} + \nabla \cdot (\alpha_s \rho_s v_s v_s) \tag{22}$$

$$= -\alpha_s \nabla p - \nabla p_s + \nabla \cdot \overline{\overline{\tau_s}} + K_{gs}(v_g - v_s) + \alpha_s \rho_s \vec{g} + \sum_{r=1;r \neq s}^{ns} K_{sr}(v_r - v_s)$$

where ns is the number of considered solid phases, p is pressure, p_s is solid phase granular pressure (*i.e.,* the pressure exerted by particles on vessel walls), K_{gs} is the gas-solid momentum exchange coefficient, K_{rs} is the solid-solid momentum exchange coefficient and g is gravitational acceleration. K_{gs} and K_{rs} can be evaluated through suitable correlations [135].

The terms $\bar{\bar{\tau}}_g$ and $\bar{\bar{\tau}}_s$ are stress-strain tensors for solid and gas phase, respectively, which can be expressed as follows:

$$\bar{\bar{\tau}}_g = \alpha_g \mu_g \left(\nabla v_g + \nabla v_g^T \right) - \frac{2}{3} \alpha_g \mu_g \cdot (\nabla \cdot v_g) \bar{\bar{I}} \tag{23}$$

$$\bar{\bar{\tau}}_s = \alpha_s \mu_s (\nabla v_s + \nabla v_s^T) + \alpha_s \left(\lambda_s - \frac{2}{3} \mu_s \right) \cdot (\nabla \cdot v_s) \bar{\bar{I}} \tag{24}$$

where μ_g is gas viscosity, μ_s is solid shear viscosity, λ_s is solid bulk viscosity and $\bar{\bar{I}}$ is identity matrix.

Although the solid phases are modeled as a fluid, it must be taken into account that their behavior is heavily influenced by the presence of particle-particle collisions; such effect must be included in the estimation of p_s, μ_s and λ_s, which can be carried out by means of the kinetic theory of granular flow [136].

Energy balances for the gas phase and each solid phase can be written as follows:

$$\frac{\partial}{\partial t} (\alpha_g \rho_g h_g) + \nabla \cdot (\alpha_g \rho_g h_g v_g) = -\alpha_g \frac{\partial P_g}{\partial t} - \nabla \cdot q_g + \bar{\bar{\tau}}_g : \nabla v_g + \sum_{r=1}^{ns} (Q_{rg} - \dot{m}_{rg} h_{rg}) \tag{25}$$

$$\frac{\partial}{\partial t} (\alpha_s \rho_s h_s) + \nabla \cdot (\alpha_s \rho_s h_s v_s) = -\alpha_s \frac{\partial P_s}{\partial t} - \nabla \cdot q_s + \bar{\bar{\tau}}_s : \nabla v_s - Q_{sg} + \dot{m}_{gs} h_{gs} + \Delta Q_r \tag{26}$$

where h_g and h_s are the enthalpy of the gas and solid phase, respectively, h_{gs} is the enthalpy related to the interphase gas-solid flow, q_g and q_s are heat fluxes of gas and solid phase, respectively, Q_{sg} is the intensity of heat exchange between gas and solid phases and ΔQ_r is the heat production rate due to the exothermic polymerization reaction. In particular, the heat flux is computed according to Fourier's law; the thermal conductivity of the solid phase can be estimated through the kinetic theory of granular flow.

PBE are employed to evaluate the polydisperse population of solid particles, since all those phenomena that influence the particle size distribution (PSD) in the reactor can be properly accounted for. Indeed, the PSD in a given region of the vessel is not only determined by the presence of the flow field that makes particles move according to their size, but also by aggregation and breakage phenomena and above all by the particle growth due to polymerization

kinetics. Assuming that only the particle size L is employed as internal coordinate, PBE can be written as follows [137]:

$$\frac{\partial n(L;\,x,t)}{\partial t} + \nabla \cdot [v_s n(L;\,x,t)] = -\frac{\partial}{\partial L}[G(L)n(L;\,x,t)] + B_{ag}(L;\,x,t) - D_{ag}(L;\,x,t) +$$
$$B_{br}(L;\,x,t) - D_{br}(L;\,x,t) \tag{27}$$

where $n(L;\,x,t)$ is the number density function for particles with size L, in a given point of coordinates x at time t, $G(L)$ is the growth rate due to polymerization kinetics, B_{ag} and D_{ag} are the birth and death rates due to particle aggregation, respectively, and B_{br} and D_{br} are the birth and death rates due to particle aggregation, respectively. Birth and death rates can be written as follows [138] :

$$B_{ag}(L;x,t) = \frac{L^2}{2}\int_0^L \frac{\beta((L^3-\lambda^3)^{\frac{1}{3}},\lambda)}{(L^3-\lambda^3)^{\frac{2}{3}}} n((L^3-\lambda^3)^{\frac{1}{3}};x,t)n(\lambda;x,t)d\lambda \tag{28}$$

$$D_{ag}(L;x,t) = n(L;x,t)\int_0^\infty \beta(L,\lambda)n(\lambda;x,t)d\lambda \tag{29}$$

$$B_{br}(L;x,t) = \int_L^\infty a(\lambda)b(L|\lambda)n(\lambda;x,t)d\lambda \tag{30}$$

$$D_{br}(L;x,t) = a(L)n(L;x,t) \tag{31}$$

where λ is particle size, $\beta(L,\lambda)$ is the aggregation kernel, $a(L)$ is breakage kernel and $b(L|\lambda)$ is the daughter distribution function. While there are well-established expressions for the polymerization kinetics (that can also include the amount of catalyst active sites and their dynamic deactivation), aggregation and breakage phenomena require a suitable kernel to be included [137], [139].

Since the numerical solution of PBE can be challenging and expensive from a computational point of view, many approaches were developed in order to solve this issue. The most employed ones are quadrature based moments methods, such as the quadrature method of moments (QMOM) and the direct quadrature method of moments (DQMOM), which constitutes a simplification of the original QMOM approach [140].

4.1.1 Applications

As anticipated, the use of CFD simulations represents an attractive way to achieve accurate information about the process (gas and solid velocity fields, solid distribution in the reactor, temperature profile, et cetera), which are not always accessible experimentally because of the invasive measurements needed and the challenging operative conditions of the FBR (in terms of temperature, pressure and solid volume fraction). In this regard, they act as a computer experiment that allows measuring the properties of interest with high spatiotemporal resolution.

Fluidized bed reactors are often modelled adopting pseudo two-dimensional geometries, for the sake of computational efficiency. Indeed, despite the improvements that involved both hardware and software, multiphase simulations can be still expensive from a computational point of view.

Focusing on boundary conditions, gas velocity is fixed at the inlet, while a pressure boundary condition is imposed at the outlet; no-slip condition is set at reactor walls for gas phase, while no-slip or partial slip is applied for solid phases. In most cases solid content is fixed, i.e., neither inlet nor outlet for particle flow are included in the system. Simulations aim at exploring with in silico experiments the impact of operative conditions on, *e.g.*, fluidization, solid segregation and temperature through parametric calculations. Model validation is usually carried out by comparing the predicted pressure drops and/or the bed axial height with experimental data (from lab scale reactors to industrial plants).

Just for curiosity, up to authors' best knowledge the biggest computational effort for CFD applied to a fluidized bed reactor was recently reported by Neau *et al.* [141], who employed 36,000 CPU cores, a mesh composed of a billion element and 15 millions of CPU hours to simulate an industrial scale FBR with a three-dimensional geometry. Even though the calculation produced 200 TB of data, the simulated physical time was no longer than 25 s.

Akbari *et al.* [142], [143] performed parametric simulations of an industrial scale fluidized bed reactor. First, they focused their attention on the numerical solution scheme, validating the model by comparing the calculated pressure drops with plant data. The authors subsequently analyzed the effect of the minimum fluidization velocity and particle growth rate on fluidization behavior and solid segregation.

Che *et al.* [144], [145] performed a more detailed analysis, which involved a pilot-plant scale FBR for ethylene polymerization. After investigating the impact of particle size and gas velocity on fluidization, the authors employed population balance equations including not only polymerization kinetics but also aggregation and breaking phenomena. Results showed that particle growth due to polymerization has a remarkable influence on flow fields and solid distribution in the reactor; moreover, particle breakage led to a reduction of average particle size and to an increased axial expansion of the bed. The same research group [146] further improved the model by adopting a three-dimensional schematization of the reactor; validation was carried out by comparing pressure drops and bed axial height.

There are also some attempts to employ CFD simulations in order to compute the residence time distribution (RTD) of the solid [147], [148], using monodisperse non-reacting and non-interacting particles (*i.e.*, neither aggregation nor breakage take place). In this case, reactor geometry also included an inlet and an outlet for the solid phase; when steady state was reached, a tracer pulse was added and its outlet flow was monitored in order to compute RTD directly from its definition.

Khan *et al.* [149] implemented a dynamic multiphase model (that accounts for both emulsion and bubble phase) within a CFD Eulerian model. The modeling framework was validated with experimental data obtained from a lab scale reactor and employed to identify the optimal range of operative conditions.

Bumphenkiattikul *et al.* [150] coupled a phenomenological mathematical model and CFD simulations for the analysis of hot spots and heat transfer in FBR reactors. Both models included population balances for the implementation of detailed kinetic scheme for polymerization (that involved initiation, propagation, chain transfer and termination) subsequently solved with the method of the moments.

The developed scheme is the following: CFD simulations focused on hydrodynamics were employed to obtain solid holdup and heat transfer coefficients that were included in the phenomenological model, which was subsequently used to compute the steady state regime of the reactor (in terms of temperature, monomer and catalyst concentration, moments for living and dead chains, et cetera). This, in turn, was the starting point for comprehensive CFD simulations.

The aim of such computational protocol was to obtain an agile way for a reliable estimation of the steady state regime, which can be challenging to achieve directly with CFD due to the required computational time and numerical issues. Overall, the authors provided useful insights about the scale-up of FBR reactors from lab scale to pilot plant scale.

Zhu *et al.* [16] proposed a multiscale approach by implementing a single particle model (in essence, a polymeric flow model) in a CFD simulation. Such model is composed of both mass and energy conservation equations, written at steady state and considering only radial coordinate for concentration and temperature gradients. This multiscale model was employed to assess the influence of interphase mass and energy transport. Simulation outcomes confirmed the major role of intraparticle mass transfer, while intraparticle heat transfer could be neglected.

Schneiderbauer *et al.* [151] developed a computational approach for the coarse grid simulation of industrial scale reactors (which could not be investigated otherwise) and validated it with lab scale data. The authors subsequently simulated the behavior of an industrial scale system composed of a fluidized bed reactor and a moving bed reactor, as depicted in Figure 1111a; contour plots of solid volume fractions are given in Figure 1111b.


a)
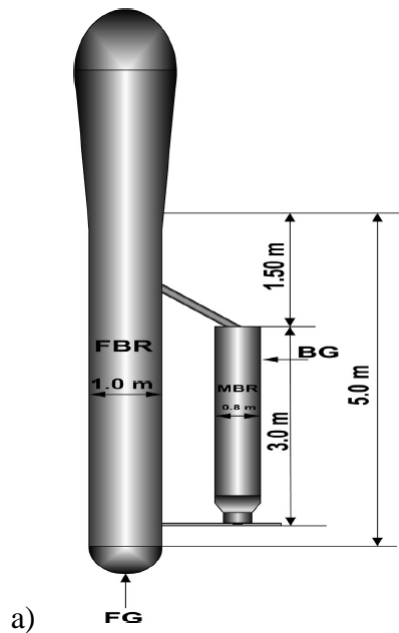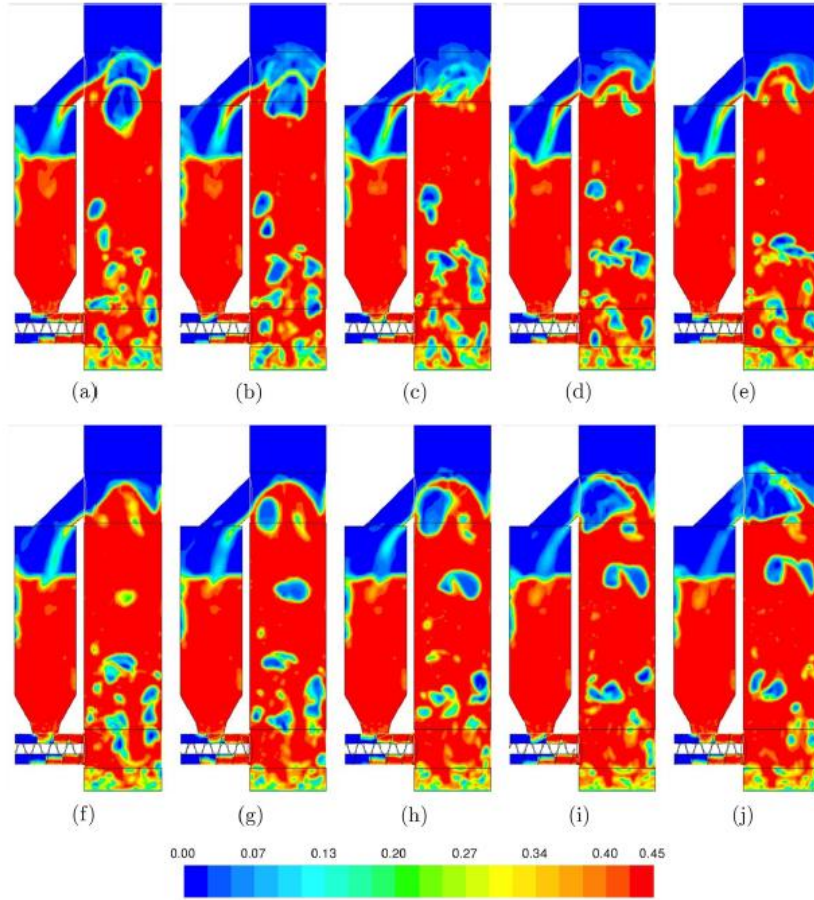
b)

Figure 11. Schematic of the investigated industrial scale reactor (a). Solid phase volume fraction inside the vessels at steady state; snapshots were taken every 0.1 s of physical simulated time (b). Reproduced with permission from Schneiderbauer *et al.* [151]. Copyright 2014 Elsevier.

Yao *et al.* [152] performed a parametric analysis investigating the influence of the employed drag model on FBR simulations. The authors found that the chosen correlation had a concrete impact on bed height, temperature and solid phase segregation but a little influence on the evolution of Sauter diameter and PSD. Overall, they recommended the energy minimization multiscale (EMMS) model, which includes a correction factor that takes into account the reduction of drag coefficient due to particle aggregation. Yao *et al.* [153] systematically analyzed also the performances of three commonly employed quadrature based moments methods for the PBE solution that included particle growth, breakage and aggregation: QMOM, DQMOM and fixed pivot quadrature method of the moments (FPQMOM). According to their outcomes, the author recommended the use of FPQMOM.

CFD simulations of FBR are also employed to address the problem of wall coating formation due to the tribocharging of ethylene particles [154], [155]. Ray *et al.* [156] developed an Eulerian model that includes particle charging due to particle-particle and particle-wall collision. Model results allow computing electrostatic potential and electric field strength as a function of time and space in the reactor, as shown in 12a for 362 μm particles after 10 s of simulated physical time, and the size-dependent particle charging (Figure 1212b). Results were consistent with experimental findings; in particular, the outcomes suggested that particles bigger than 425 μm are not able to stick to the wall, in qualitative agreement with the 600 μm value suggested by experiments.
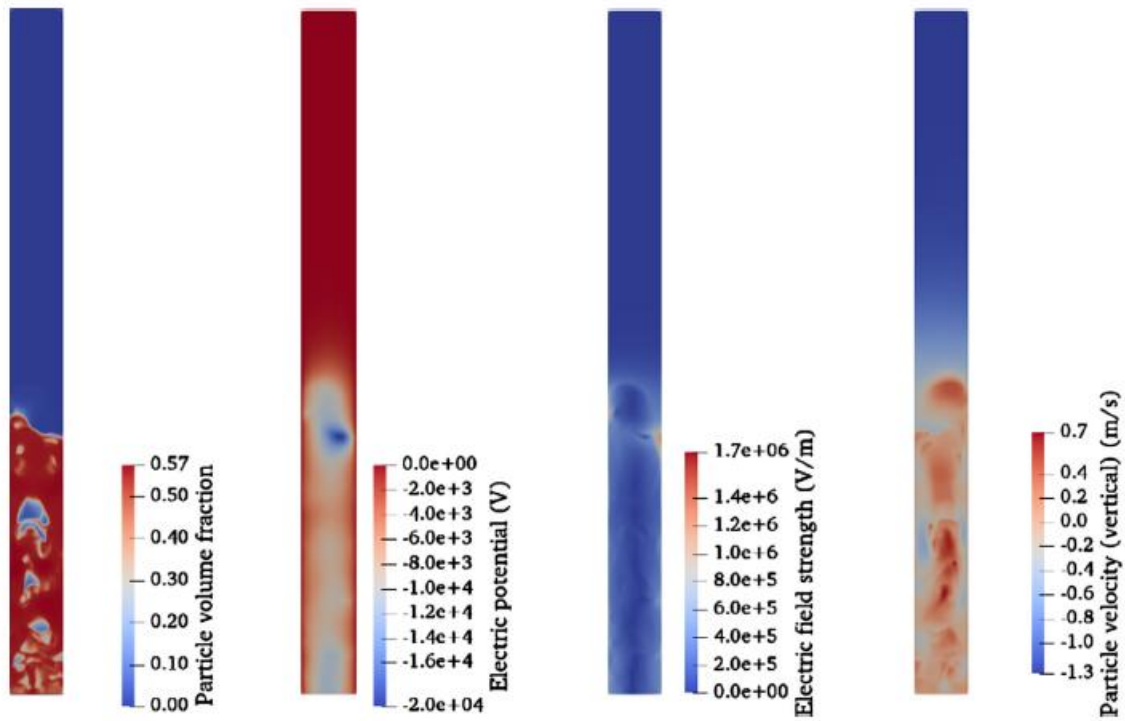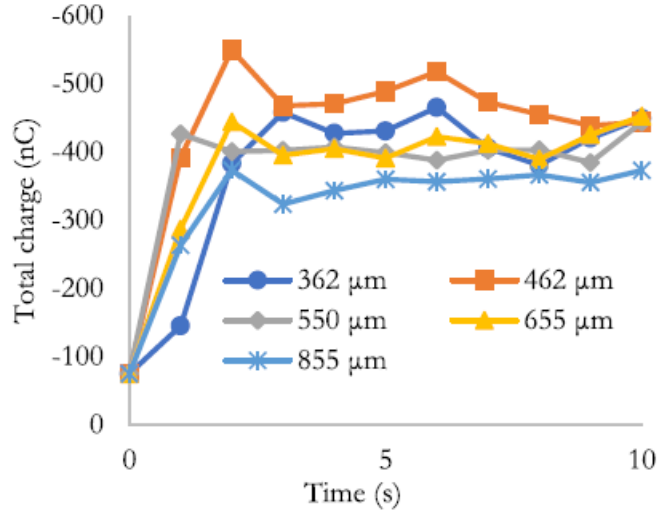
Figure 12. Particle volume fraction, electric potential, electric field strength and particle velocity in the reactor after 10 s of simulated physical time with a monodisperse 362 μm diameter particle population (a). Time evolution of total bed charge as a function of the inlet particle size (b). Reproduced with permission from Ray *et al.* [156]. Copyright 2019 Elsevier

The authors also pointed out that, despite the promising results, a sensitivity analysis for the employed parameters will be performed; indeed, the steady state was reached in about 4 seconds in the simulations, while the experimental setup needs about 15 minutes, suggesting that charge diffusion was accelerated in the performed calculations.

4.1.2 Focus on condensed mode simulations

The Euler model proved to be a suitable approach to investigate the behavior of FBR under condensed mode operation. The presence of droplets can be accounted for by adding a liquid phase in the system and modifying the constitutive laws accordingly as proposed, *e.g.*, by Pan *et al.* [157]. Continuity equations can be written as follows:

$$\frac{\partial \alpha_g \rho_g}{\partial t} + \nabla \cdot (\alpha_g \rho_g v_g) = \dot{m}_{lg} - \dot{m}_{gs} \tag{32}$$

$$\frac{\partial \alpha_s \rho_s}{\partial t} + \nabla \cdot (\alpha_s \rho_s v_s) = \dot{m}_{gs} \tag{33}$$

$$\frac{\partial \alpha_l \rho_l}{\partial t} + \nabla \cdot (\alpha_l \rho_l v_l) = -\dot{m}_{lg} \tag{34}$$

where the subscript l is referred to the liquid phase; in particular, $\dot{m}_{lg}$ represents the mass transfer from the liquid to gas phase due to evaporation. Momentum conservation equations can be written as follows:

$$\frac{\partial \alpha_g \rho_g v_g}{\partial t} + \nabla \cdot (\alpha_g \rho_g v_g v_g) = -\alpha_g \nabla p + \nabla \cdot \overline{\overline{\tau_g}} + \alpha_g \rho_g g + \sum_{r=1}^{ns} K_{gr}(v_r - v_g) - \dot{m}_{gs} v_g + \tag{35}$$

$$\dot{m}_{lg} v_l + K_{lg}(v_l - v_g)$$

$$\frac{\partial \alpha_s \rho_s v_s}{\partial t} + \nabla \cdot (\alpha_s \rho_s v_s v_s) \tag{36}$$

$$= -\alpha_s \nabla p - \nabla p_s + \nabla \cdot \overline{\overline{\tau}}_s + K_{gs}(v_g - v_s) + \alpha_s \rho_s \vec{g}$$

$$+ \sum_{r=1;r \neq s}^{ns} K_{sr}(v_r - v_s) + K_{ls}(v_l - v_s)$$

$$\frac{\partial \alpha_l \rho_l v_l}{\partial t} + \nabla \cdot (\alpha_l \rho_l v_l v_l) = -\alpha_l \nabla p + \nabla \cdot \overline{\overline{\tau}}_l + \alpha_l \rho_l g + \sum_{r=1}^{ns} K_{lr}(v_r - v_l) + -\dot{m}_{lg} v_l + \tag{37}$$

$$K_{lg}(v_g - v_l)$$

where K_{lg} and K_{ls} are interphase momentum exchange coefficients between the liquid and the gas phase and between the liquid and the solid phase, respectively; they can be estimated with existing correlation as mentioned above (*vide supra*). Stress tensor for liquid phase can be written as shown in eq. 25, adopting appropriate values for the physical constants.

Energy balances have the following form:

$$\frac{\partial}{\partial t}(\alpha_g \rho_g h_g) + \nabla \cdot (\alpha_g \rho_g h_g v_g) = -\alpha_g \frac{\partial P_g}{\partial t} - \nabla \cdot q_g + \overline{\overline{\tau}}_g : \nabla v_g + \sum_{r=1}^{ns}(Q_{rg} - \dot{m}_{rg} h_{rg}) + \tag{38}$$

$$Q_{lg} + \dot{m}_{lg} h_{lg}$$

$$\frac{\partial}{\partial t}(\alpha_s \rho_s h_s) + \nabla \cdot (\alpha_s \rho_s h_s v_s) = -\alpha_s \frac{\partial P_s}{\partial t} - \nabla \cdot q_s + \overline{\overline{\tau}}_s : \nabla v_s - Q_{sg} + \dot{m}_{gs} h_{gs} + \Delta Q_r \tag{39}$$

$$\frac{\partial}{\partial t}(\alpha_l \rho_l h_l) + \nabla \cdot (\alpha_l \rho_l h_l v_l) = -\alpha_l \frac{\partial P_l}{\partial t} - \nabla \cdot q_l + \overline{\overline{\tau}}_l : \nabla v_l - Q_{lg} - \dot{m}_{lg} h_{lg} - \dot{m}_{lg} \Delta H_{vap} \tag{40}$$

where Q_{lg} is the is the intensity of heat exchange between gas and liquid phases and ΔH_{vap} is the enthalpy of vaporization of the added inert. Pan *et al.* [158] also developed and implemented a model for the vaporization of the liquid, explicitly accounting for the presence of a polydisperse

population of droplets. The overall modeling framework was validated with industrial data, in terms of reactor temperature at different height values.

The authors subsequently employed such three-phase model, along with the droplet vaporization model [159], [160] and a comprehensive kinetic scheme, to evaluate the impact of the amount of isopentane on reactor behavior. Although the dynamic variation of the gas heat capacity due to droplet evaporation and the increased monomer solubility in the polymer were not accounted for, CFD simulation outcomes showed a decrease in bed mean temperature as a function of the inlet concentration of isopentane, as depicted in Figure 133. Simulations also showed an enhanced polyethylene production rate and therefore an increased solid volume fraction (again in Figure 133); although this effect can be counterintuitive due to the lower bed temperature, it can be due to the temperature-dependent interplay of propagation and catalyst deactivation kinetics.
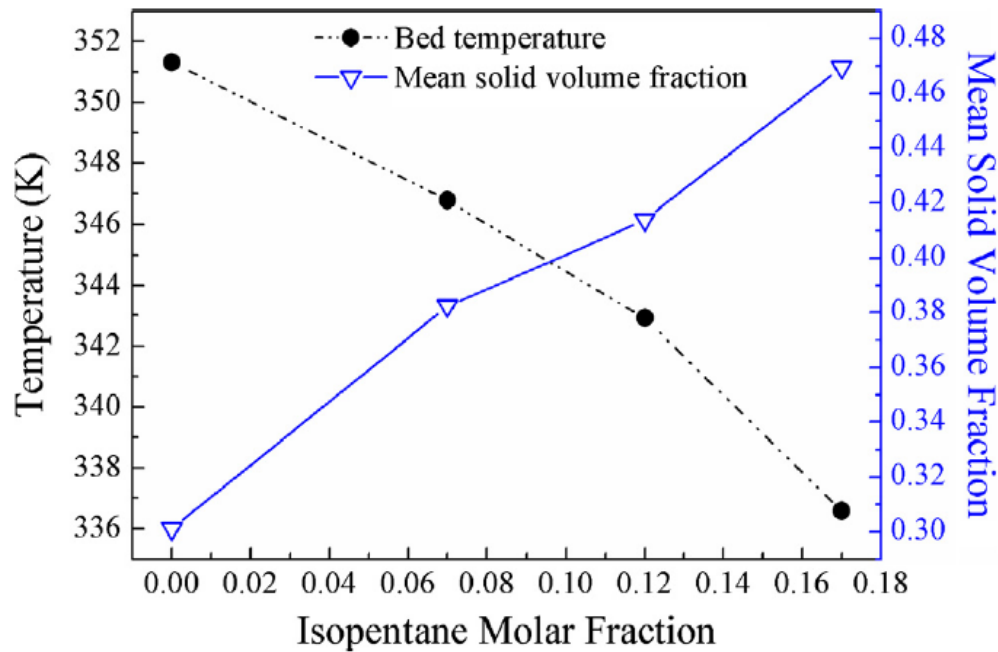

Figure 13. Mean bed temperature and solid volume fraction as a function of the molar fraction of isopentane. Reproduced with permission from Pan *et al.* [157] Copyright 2016 The Society of Powder Technology Japan.

5   Conclusions

This review focused on the main macroscale approaches to modelling a FBR for PE production. For non-CFD models, 3 main approaches have been discussed and comparative studies show that they all have specific uses. The one phase, well-mixed approach is of mathematical simplicity, and when coupled with a kinetic model, one can obtain basic results such as production rate, monomer conversion, and depending on the kinetic model, molecular weight and composition distributions. The biggest downside of this model is the lack of rigor when describing the heat and mass transfer between gas and solid phases. This issue can be overcome by finely tuning model parameters for each specific case. However, this procedure would result in strongly system-dependent parameter values, which, in turn, negatively affect the predictive capability of the model for different process conditions. The two-phase approach is divided into constant and variable bubble size models. The first, is not physically accurate, and comparative studies show little to no improvement when adding a bubble phase against a one phase, well mixed approach. This might be related to how heavily the two-phase models depend on the use of empirical or semi-empirical correlations for key reactor parameters, such as the bubble volume fraction, the bubble size, interphase mass and heat transfer coefficients, etc. The two-phase variable bubble size model shows promising results, most likely due their more accurate description of heat and mass transfer between bubbles, but at the expense of even correlations than the constant bubble size. In all of these approaches, there is an array of available models that range from simple to very detailed and complex. Depending on the results that are required, one can choose the level of complexity.

In terms of the studies found in the literature, a good balance between homo- and co-polymerization studies was observed. However, most studies focus on dry-mode or dismiss co-solubility effects all together, which goes against what is practiced in the industry.

The use of CFD models proved to provide useful results and emerged as a promising approach by virtue of their spatiotemporal resolution, which allows obtaining insights about velocity fields and temperature profiles that would be challenging or impossible to investigate otherwise. Anyway, CFD simulations for FBR still require some simplifications for the computational efficiency (the solid is treated as a continuum) and are currently at their infancy, since they are mainly employed to characterize bed fluidization. The direct evaluation of particle size

distribution as well as molecular weight distribution currently lacks a comprehensive validation; while condensed mode operation was simulated, co-solubility effects were ignored. Given the proven potential of CFD and the continuous advancements concerning both hardware and software, an increased implementation of CFD-based tools and an ever-growing descriptive capability for FBR simulations are envisaged in the near future.

Acknowledgementss

6   Bibliography

[1]   J. B. P. Soares and T. F. L. McKenna, *Polyolefin Reaction Engineering*. Wiley-VCH, 2012.

[2]   D. Kunii and O. Levenspiel, *Fluidization Engineering*, 2nd Editio. Butterworth-Heinemann, 1991.

[3]   A. R. Secchi, G. A. Neumann, and R. Gambetta, "Gas Fluidized Bed Polymerization," in *Fluidization Engineering: Practice*, Second Exp., M. L. Passos, M. A. S. Barrozo, and A. S. Mujumdar, Eds. 2014, pp. 59–95.

[4]   M. Covezzi and G. Mei, "The multizone circulating reactor technology," *Chem. Eng. Sci.*, vol. 56, no. 13, pp. 4059–4067, Aug. 2001, doi: 10.1016/S0009-2509(01)00077-X.

[5]   T. F. L. McKenna, "Condensed Mode Cooling of Ethylene Polymerization in Fluidized Bed Reactors," *Macromolecular Reaction Engineering*, vol. 13, no. 2. p. 1800026, Apr. 15, 2019, doi: 10.1002/mren.201800026.

[6]   A. Bragança, A. Morschbacker, E. Rubbo, C. Miro, T. Barlem, and A. Mukherjee, "Process for the gas phase polymerization and copolymerization of olefin monomers," US 6864332 B2, 2005.

[7]   A. Alizadeh and T. F. L. McKenna, "Condensed mode cooling in ethylene polymerisation:

droplet evaporation," *Macromol. Symp.*, vol. 333, no. 1, pp. 242–247, Nov. 2013, doi: 10.1002/masy.201300092.

[8]   K. K. Botros, G. Price, V. Ker, Y. Jiang, and S. K. Goyal, "Effects of hydrocarbon liquid feed in polyethylene polymerization process on particle surface temperature," *Chem. Eng. Commun.*, vol. 193, no. 12, pp. 1612–1634, Dec. 2006, doi: 10.1080/00986440600586511.

[9]   M. Namkajorn, A. Alizadeh, E. Somsook, and T. F. L. McKenna, "Condensed Mode Cooling for Ethylene Polymerisation : The Influence of Inert Condensing Agent on the Polymerisation Rate," *Macromol. Chem. Phys.*, vol. 215, no. 9, pp. 873–878, 2014.

[10] A. Alizadeh, M. Namkajorn, E. Somsook, and T. F. L. McKenna, "Condensed Mode Cooling for Ethylene Polymerization: Part I. The Effect of Different Induced Condensing Agents on Polymerization Rate," *Macromol. Chem. Phys.*, vol. 216, no. 8, pp. 903–913, 2015.

[11] A. Alizadeh, M. Namkajorn, E. Somsook, and T. F. L. McKenna, "Condensed Mode Cooling for Ethylene Polymerization: Part II. From Cosolubility to Comonomer and Hydrogen Effects," *Macromol. Chem. Phys.*, vol. 216, no. 9, pp. 985–995, 2015.

[12] A. Wonders, G. E. Moore, R. R. Ford, F. D. Daily, K. A. Dooley, and J. J. Garcia, "Suppression of Fines in Fluid Bed Polyethylene Process," Patent US 5969061, 1999.

[13] V. Kanellopoulos, D. Mouratides, E. Tsiliopoulou, and C. Kiparissides, "An Experimental and Theoretical Investigation into the Diffusion of Olefins in Semi-Crystalline Polymers: The Influence of Swelling in Polymer-Penetrant Systems," *Macromol. React. Eng.*, vol. 1, no. 1, pp. 106–118, 2007.

[14] V. Touloupidis, "Catalytic Olefin Polymerization Process Modeling: Multi-Scale Approach and Modeling Guidelines for Micro-Scale/Kinetic Modeling," *Macromol. React. Eng.*, vol. 8, no. 7, pp. 508–527, Jul. 2014, doi: 10.1002/mren.201300188.

[15] M. R. Abbasi, A. Shamiri, and M. A. Hussain, "A review on modeling and control of olefin polymerization in fluidized-bed reactors," *Reviews in Chemical Engineering*, vol. 35, no. 3. De Gruyter, pp. 311–333, Apr. 01, 2019, doi: 10.1515/revce-2017-0040.

[16] Y. P. Zhu, G. Q. Chen, and Z. H. Luo, "Particle behavior in FBRs: A comparison of the PBM-CFD, multi-scale CFD simulation of gas-solid catalytic propylene polymerization," *Macromol. React. Eng.*, vol. 8, no. 9, pp. 609–621, Sep. 2014, doi: 10.1002/mren.201300196.

[17]   T. Xie, K. B. McAuley, J. C. C. Hsu, and D. W. Bacon., "Gas phase ethylene polymerization: Production processes, polymer properties, and reactor modeling," *Ind. Eng. Chem. Res.*, vol. 33, no. 3, pp. 449–479, 1994.

[18]   C. Kiparissides, "Polymerization reactor modeling: A review of recent developments and future directions," *Chem. Eng. Sci.*, vol. 51, no. 10, pp. 1637–1659, 1996, doi: 10.1016/0009-2509(96)00024-3.

[19]   A. E. Hamielec and J. B. P. Soares, "Polymerization reaction engineering - Metallocene catalysts," *Progress in Polymer Science (Oxford)*, vol. 21, no. 4. Elsevier Ltd, pp. 651–706, 1996, doi: 10.1016/0079-6700(96)00001-9.

[20]   J. Sun *et al.*, "Important mesoscale phenomena in gas phase fluidized bed ethylene polymerization," *Particuology*, vol. 48, pp. 116–143, Feb. 2020, doi: 10.1016/j.partic.2018.12.004.

[21]   Y. Kaneko, T. Shiojima, and M. Horio, "DEM simulation of fluidized beds for gas-phase olefin polymerization," *Chem. Eng. Sci.*, vol. 54, no. 24, pp. 5809–5821, Dec. 1999, doi: 10.1016/S0009-2509(99)00153-0.

[22]   T. F. L. McKenna and J. B. P. Soares, "Single particle modelling for olefin polymerization on supported catalysts: A review and proposals for future developments," *Chem. Eng. Sci.*, vol. 56, no. 13, pp. 3931–3949, Aug. 2001, doi: 10.1016/S0009-2509(01)00069-0.

[23]   T. F. L. McKenna, A. Di Martino, G. Weickert, and J. B. P. Soares, "Particle growth during the polymerisation of olefins on supported catalysts, 1 - Nascent polymer structures," *Macromolecular Reaction Engineering*, vol. 4, no. 1. John Wiley & Sons, Ltd, pp. 40–64, Jan. 08, 2010, doi: 10.1002/mren.200900025.

[24]   A. Alizadeh and T. F. L. McKenna, "Particle Growth during the Polymerization of Olefins on Supported Catalysts. Part 2: Current Experimental Understanding and Modeling Progresses on Particle Fragmentation, Growth, and Morphology Development," *Macromolecular Reaction Engineering*, vol. 12, no. 1. Wiley-VCH Verlag, p. 1700027, Feb. 01, 2018, doi: 10.1002/mren.201700027.

[25]   J. B. P. Soares, "Mathematical modelling of the microstructure of polyolefins made by coordination polymerization: A review," *Chem. Eng. Sci.*, vol. 56, no. 13, pp. 4131–4153, 2001, doi: 10.1016/S0009-2509(01)00083-5.

[26]   A. Zecchina, S. Bordiga, and E. Groppo, "The Structure and Reactivity of Single and

Multiple Sites on Heterogeneous and Homogeneous Catalysts: Analogies, Differences, and Challenges for Characterization Methods," in *Selective Nanocatalysts and Nanoscience: Concepts for Heterogeneous and Homogeneous Catalysis*, Weinheim, Germany: Wiley-VCH Verlag GmbH & Co. KGaA, 2011, pp. 1–27.

[27]   A. R. Albunia, F. Prades, and D. Jeremic, *Multimodal polymers with supported catalysts: Design and production*. Springer International Publishing, 2019.

[28]   S. Floyd, K. Y. Choi, T. W. Taylor, and W. H. Ray, "Polymerization of Olefins through Heterogeneous Catalysis III. Polymer Particle Modelling with an Analysis of Intraparticle Heat and Mass Transfer Effects," *J. Appl. Polym. Sci*, vol. 32, no. 1, pp. 2935–2960, 1986.

[29]   S. Floyd, "A theoretical interpretation of reactivity ratio products in copolymers formed from two fractions differing in composition," *J. Appl. Polym. Sci.*, vol. 34, no. 7, pp. 2559–2574, Nov. 1987, doi: 10.1002/app.1987.070340719.

[30]   Y. V. Kissin, "Kinetics of olefin copolymerization with heterogeneous Ziegler- Natta catalysts," *Macromol. Symp.*, vol. 89, no. 1, pp. 113–123, Jan. 1995, doi: 10.1002/masy.19950890113.

[31]   Y. V. Kissin, R. I. Mink, and T. E. Nowlin, "Ethylene polymerization reactions with Ziegler-Natta catalysts. I. Ethylene polymerization kinetics and kinetic mechanism," *J. Polym. Sci. Part A Polym. Chem.*, vol. 37, no. 23, pp. 4255–4272, Dec. 1999, doi: 10.1002/(SICI)1099-0518(19991201)37:23<4255::AID-POLA2>3.0.CO;2-H.

[32]   Y. V. Kissin and A. J. Brandolini, "Ethylene polymerization reactions with Ziegler-Natta catalysts. II. Ethylene polymerization reactions in the presence of deuterium," *J. Polym. Sci. Part A Polym. Chem.*, vol. 37, no. 23, pp. 4273–4280, Dec. 1999, doi: 10.1002/(SICI)1099-0518(19991201)37:23<4273::AID-POLA3>3.0.CO;2-A.

[33]   Y. V. Kissin, "Main kinetic features of ethylene polymerization reactions with heterogeneous Ziegler-Natta catalysts in the light of a multicenter reaction mechanism," *J. Polym. Sci. Part A Polym. Chem.*, vol. 39, no. 10, pp. 1681–1695, May 2001, doi: 10.1002/pola.1146.

[34]   Y. V. Kissin, "Multicenter nature of titanium-based Ziegler-Natta catalysts: Comparison of ethylene and propylene polymerization reactions," *J. Polym. Sci. Part A Polym. Chem.*, vol. 41, no. 12, pp. 1745–1758, Jun. 2003, doi: 10.1002/pola.10714.

[35]   M. M. Ranieri, J. P. Broyer, F. Cutillo, T. F. L. McKenna, and C. Boisson, "Site count: Is a

high-pressure quenched-flow reactor suitable for kinetic studies of molecular catalysts in ethylene polymerization?," *Dalt. Trans.*, vol. 42, no. 25, pp. 9049–9057, Jul. 2013, doi: 10.1039/c3dt33004d.

[36] T. F. L. McKenna, E. Tioni, M. M. Ranieri, A. Alizadeh, C. Boisson, and V. Monteil, "Catalytic olefin polymerisation at short times: Studies using specially adapted reactors," *Can. J. Chem. Eng.*, vol. 91, no. 4, pp. 669–686, Apr. 2013, doi: 10.1002/cjce.21684.

[37] T. F. L. McKenna, C. Boisson, V. Monteil, E. Ranieri, and E. Tioni, "Specialised tools for a better comprehension of olefin polymerisation reactors," *Macromol. Symp.*, vol. 333, no. 1, pp. 233–241, Nov. 2013, doi: 10.1002/masy.201300076.

[38] S. K. GUPTA, "Low density polyethylene (LDPE) polymerization — A review," *Curr. Sci.*, vol. 56, no. 19, pp. 979–984, 1987.

[39] T. McKenna and V. Mattioli, "Progress in describing particle growth for polyolefins: A look at particle morphology," in *Macromolecular Symposia*, Aug. 2001, vol. 173, no. 1, pp. 149–162, doi: 10.1002/1521-3900(200108)173:1<149::AID-MASY149>3.0.CO;2-E.

[40] P. Kittilsen, T. F. McKenna, H. Svendsen, H. A. Jakobsen, and S. B. Fredriksen, "The interaction between mass transfer effects and morphology in heterogeneous olefin polymerization," *Chem. Eng. Sci.*, vol. 56, no. 13, pp. 4015–4028, Aug. 2001, doi: 10.1016/S0009-2509(01)00074-4.

[41] A. Di Martino, G. Weickert, F. Sidoroff, and T. F. L. McKenna, "Modelling Induced Tension in a Growing Catalyst/Polyolefin Particle: A Multi-Scale Approach for Simplified Morphology Modelling," *Macromol. React. Eng.*, vol. 1, no. 3, pp. 338–352, May 2007, doi: 10.1002/mren.200600036.

[42] T. F. L. McKenna, "Growth and evolution of particle morphology: An experimental & modelling study," *Macromol. Symp.*, vol. 260, no. 1, pp. 65–73, Dec. 2007, doi: 10.1002/masy.200751410.

[43] Z. Grof, J. Kosek, M. Marek, and P. M. Adler, "Modeling of morphogenesis of polyolefin particles: Catalyst fragmentation," *AIChE J.*, vol. 49, no. 4, pp. 1002–1013, Apr. 2003, doi: 10.1002/aic.690490417.

[44] B. Horáčková, Z. Grof, and J. Kosek, "Dynamics of fragmentation of catalyst carriers in catalytic polymerization of olefins," *Chem. Eng. Sci.*, vol. 62, no. 18–20, pp. 5264–5270, Sep. 2007, doi: 10.1016/j.ces.2007.03.022.

[45] Z. Grof, J. Kosek, and M. Marek, "Principles of the morphogenesis of polyolefin particles," *Ind. Eng. Chem. Res.*, vol. 44, no. 8, pp. 2389–2404, Feb. 2005, doi: 10.1021/ie049106j.

[46] Z. Grof, J. Kosek, and M. Marek, "Modeling of morphogenesis of growing polyolefin particles," in *AIChE Journal*, Jul. 2005, vol. 51, no. 7, pp. 2048–2067, doi: 10.1002/aic.10549.

[47] D. A. Estenoz and M. G. Chiovetta, "A structural model for the catalytic polymerization of ethylene using chromium catalysts. Part I: Description and solution," *Polym. Eng. Sci.*, vol. 36, no. 17, pp. 2208–2228, Sep. 1996, doi: 10.1002/pen.10618.

[48] D. A. Estenoz and M. G. Chiovetta, "Olefin polymerization using supported metallocene catalysts: Process representation scheme and mathematical model," *J. Appl. Polym. Sci.*, vol. 81, no. 2, pp. 285–311, 2001, doi: 10.1002/app.1440.

[49] A. G. Fisch, J. H. Z. Dos Santos, A. R. Secchi, and N. S. M. Cardozo, "Heterogeneous Catalysts for Olefin Polymerization: Mathematical Model for Catalyst Particle Fragmentation," *Ind. Eng. Chem. Res.*, vol. 54, no. 48, pp. 11997–12010, 2015, doi: 10.1021/acs.iecr.5b03740.

[50] A. Alizadeh, J. Chmelař, F. Sharif, M. Ebrahimi, J. Kosek, and T. F. L. McKenna, "Modeling Condensed Mode Operation for Ethylene Polymerization: Part I. Thermodynamics of Sorption," *Ind. Eng. Chem. Res.*, vol. 56, no. 5, pp. 1168–1185, Feb. 2017, doi: 10.1021/acs.iecr.6b04288.

[51] A. Alizadeh, F. Sharif, M. Ebrahimi, and T. F. L. McKenna, "Modeling Condensed Mode Operation for Ethylene Polymerization: Part III. Mass and Heat Transfer," *Ind. Eng. Chem. Res.*, vol. 57, no. 18, pp. 6097–6114, May 2018, doi: 10.1021/acs.iecr.8b00330.

[52] N. Wakao and J. M. Smith, "Diffusion and reaction in porous catalysts," *Ind. Eng. Chem. Fundam.*, vol. 3, no. 2, pp. 123–127, May 1964, doi: 10.1021/i160010a007.

[53] V. Kanellopoulos, E. Tsiliopoulou, G. Dompazis, V. Touloupides, and C. Kiparissides, "Evaluation of the internal particle morphology in catalytic gas-phase olefin polymerization reactors," *Ind. Eng. Chem. Res.*, vol. 46, no. 7, pp. 1928–1937, 2007, doi: 10.1021/ie060721s.

[54] V. Kanellopoulos, G. Dompazis, B. Gustafsson, and C. Kiparissides, "Comprehensive analysis of single-particle growth in heterogeneous olefin polymerization: The random-

pore polymeric flow model," *Ind. Eng. Chem. Res.*, vol. 43, no. 17, pp. 5166–5180, 2004, doi: 10.1021/ie030810u.

[55]   S. Floyd, K. Y. Choi, T. W. Taylor, and W. H. Ray, "Polymerization of Olefins Through Heteregeneous Catalysis IV. Modeling of Heat and Mass Transfer Resistance in the Polymer Particle Boundary Layer," *J. Appl. Polym. Sci*, vol. 31, no. 7, pp. 2231–2265, 1986.

[56]   A. Yiagopoulos, H. Yiannoulakis, V. Dimos, and C. Kiparissides, "Heat and mass transfer phenomena during the early growth of a catalyst particle in gas-phase olefin polymerization: The effect of prepolymerization temperature and time," *Chem. Eng. Sci.*, vol. 56, no. 13, pp. 3979–3995, 2001, doi: 10.1016/S0009-2509(01)00071-9.

[57]   S. D. Kim and Y. Kang, "Heat and mass transfer in three-phase fluidized-bed reactors - An overview," in *Chemical Engineering Science*, 1997, vol. 52, no. 21–22, pp. 3639–3660, doi: 10.1016/S0009-2509(97)00269-8.

[58]   R. A. Hutchinson, C. M. Chen, and W. H. Ray, "Polymerization of olefins through heterogeneous catalysis X: Modeling of particle growth and morphology," *J. Appl. Polym. Sci.*, vol. 44, no. 8, pp. 1389–1414, Mar. 1992, doi: 10.1002/app.1992.070440811.

[59]   J. B. P. Soares and A. E. Hamielec, "General dynamic mathematical modelling of heterogeneous Ziegler-Natta and metallocene catalyzed copolymerization with multiple site types and mass and heat transfer resistances," *Polym. React. Eng.*, vol. 3, no. 3, pp. 261–324, 1995.

[60]   T. F. McKenna, R. Spitz, and D. Cokljat, "Heat transfer from catalysts with computational fluid dynamics," *AIChE J.*, vol. 45, no. 11, pp. 2392–2410, Nov. 1999, doi: 10.1002/aic.690451113.

[61]   J. Chang, S. Yang, and K. Zhang, "A particle-to-particle heat transfer model for dense gas-solid fluidized bed of binary mixture," *Chem. Eng. Res. Des.*, vol. 89, no. 7, pp. 894–903, 2011, doi: 10.1016/j.cherd.2010.08.004.

[62]   F. Taghipour, N. Ellis, and C. Wong, "Experimental and computational study of gas-solid fluidized bed hydrodynamics," *Chem. Eng. Sci.*, vol. 60, no. 24, pp. 6857–6867, Dec. 2005, doi: 10.1016/j.ces.2005.05.044.

[63]   C. J. Geabkoplis, *Transport Processes and Separation Process Principles*. 2006.

[64]   J. Mann, "Transport processes and unit operations," *Chem. Eng. J.*, vol. 20, no. 1, p. 82,

1980, doi: 10.1016/0300-9467(80)85013-1.

[65]   D. Kunii and O. Levenspiel, "Bubbling bed model: Model for the Flow of Gas through a Fluidized Bed," *Ind. Eng. Chem. Fundam.*, vol. 7, no. 3, pp. 446–452, Aug. 1968, doi: 10.1021/i160027a016.

[66]   D. Kunii and O. Levenspiel, "Bubbling bed model for kinetic processes in fluidized beds: Gas-Solid Mass and Heat Transfer and Catalytic Reactions," *Ind. Eng. Chem. Process Des. Dev.*, vol. 7, no. 4, pp. 481–492, 1968, doi: 10.1021/i260028a001.

[67]   A. Mahecha-Botero, J. R. Grace, S. S. E. H. Elnashaie, and C. J. Lim, "Advances in modeling of fluidized-bed catalytic reactors: A comprehensive review," *Chem. Eng. Commun.*, vol. 196, no. 11, pp. 1375–1405, 2009, doi: 10.1080/00986440902938709.

[68]   D. Ramkrishna, *Population balances : theory and applications to particulate systems in engineering*. Academic Press, 2000.

[69]   C. Kiparissides, A. Alexopoulos, A. Roussos, G. Dompazis, and C. Kotoulas, "Population balance modeling of particulate polymerization processes," in *Industrial and Engineering Chemistry Research*, Nov. 2004, vol. 43, no. 23, pp. 7290–7302, doi: 10.1021/ie049901x.

[70]   G. Dompazis, V. Kanellopoulos, and C. Kiparissides, "Assessment of particle agglomeration in catalytic olefin polymerization reactors using rheological measurements," *Ind. Eng. Chem. Res.*, vol. 45, no. 11, pp. 3800–3809, 2006, doi: 10.1021/ie051105j.

[71]   H. Hatzantonis, A. Goulas, and C. Kiparissides, "A comprehensive model for the prediction of particle-size distribution in catalyzed olefin polymerization fluidized-bed reactors," *Chem. Eng. Sci.*, vol. 53, no. 18, pp. 3251–3267, 1998, doi: 10.1016/S0009-2509(98)00122-5.

[72]   H. Arastoopour, C. S. Huang, and S. A. Weil, "Fluidization behavior of particles under agglomerating conditions," *Chem. Eng. Sci.*, vol. 43, no. 11, pp. 3063–3075, Jan. 1988, doi: 10.1016/0009-2509(88)80059-9.

[73]   M. G. Goode, M. W. Blood, and W. G. Sheard, "High Condensing Mode Polyolefin Production Under Turbulent Conditions in a Fluidized Bed," 2002.

[74]   H. Yiannoulakis, A. Yiagopoulos, and C. Kiparissides, "Recent developments in the particle size distribution modeling of fluidized-bed olefin polymerization reactors," *Chem. Eng. Sci.*, vol. 56, no. 3, pp. 917–925, Feb. 2001, doi: 10.1016/S0009-2509(00)00306-7.

[75] G. Hendrickson, "Electrostatics and gas phase fluidized bed polymerization reactor wall sheeting," *Chemical Engineering Science*, vol. 61, no. 4. pp. 1041–1064, 2006, doi: 10.1016/j.ces.2005.07.029.

[76] M. Hadisarabi, R. S. Gharebagh, R. Zarghami, and N. Mostoufi, "Computational modeling of the electrostatic charge build-up in fluidized beds," *J. Electrostat.*, vol. 97, no. October 2018, pp. 108–120, 2019, doi: 10.1016/j.elstat.2019.01.003.

[77] A. A. K. Farizhandi, H. Zhao, and R. Lau, "Modeling the change in particle size distribution in a gas-solid fluidized bed due to particle attrition using a hybrid artificial neural network-genetic algorithm approach," *Chem. Eng. Sci.*, vol. 155, pp. 210–220, Nov. 2016, doi: 10.1016/j.ces.2016.08.015.

[78] M. P. McDaniel, "Supported Chromium Catalysts for Ethylene Polymerization," *Adv. Catal.*, vol. 33, no. C, pp. 47–98, Jan. 1985, doi: 10.1016/S0360-0564(08)60258-8.

[79] G. G. Hendrickson *et al.*, "Polyolefin Reactor System Having a Gas Phase Reactor," US 9,433,914 B2, 2016.

[80] J.-R. Llinas and J.-L. Selo, "Method for reducing sheeting and agglomerates during olefin polymerisation," US 7,812,103 B2, 2010.

[81] V. Gupta, S. Singh, J. Joseph, K. J. Singala, and B. K. Desai, "Attrition resistant catalyst system for manufacture of polyolefins," US 9,605,089 B2, 2017.

[82] S. S. Lee and N. M. Karayannis, "Olefin polymerization and copolymerization catalyst," US-5223466-A, 1993.

[83] O. Ashrafi, H. Nazari-Pouya, N. Mostoufi, and R. Sotudeh-Gharebagh, "Particle size distribution in gas-phase polyethylene reactors," *Adv. Powder Technol.*, vol. 19, no. 4, pp. 321–334, 2008, doi: 10.1163/156855208X314967.

[84] K. B. McAuley, J. F. MacGregor, and A. E. Hamielec, "A kinetic model for industrial gas-phase ethylene copolymerization," *AIChE J.*, vol. 36, no. 6, pp. 837–850, Jun. 1990, doi: 10.1002/aic.690360605.

[85] D. Y. Khang and H. H. Lee, "Particle size distribution in fluidized beds for catalytic polymerization," *Chem. Eng. Sci.*, vol. 52, no. 3, pp. 421–431, 1997, doi: 10.1016/S0009-2509(97)86701-2.

[86] R. Alves, M. A. Bashir, and T. F. L. McKenna, "Modeling Condensed Mode Cooling for Ethylene Polymerization: Part II. Impact of Induced Condensing Agents on Ethylene

Polymerization in an FBR Operating in Super-Dry Mode," *Ind. Eng. Chem. Res.*, vol. 56, no. 46, pp. 13582–13593, 2017, doi: 10.1021/acs.iecr.7b02963.

[87] K. B. McAuley and J. F. MacGregor, "Optimal grade transitions in a gas phase polyethylene reactor," *AIChE J.*, vol. 38, no. 10, pp. 1564–1576, Oct. 1992, doi: 10.1002/aic.690381008.

[88] K. Y. Choi, X. Zhao, and S. Tang, "Population balance modeling for a continuous gas phase olefin polymerization reactor," *J. Appl. Polym. Sci.*, vol. 53, no. 12, pp. 1589–1597, Sep. 1994, doi: 10.1002/app.1994.070531205.

[89] C. Chatzidoukas, J. D. Perkins, E. N. Pistikopoulos, and C. Kiparissides, "Optimal grade transition and selection of closed-loop controllers in a gas-phase olefin polymerization fluidized bed reactor," *Chem. Eng. Sci.*, vol. 58, no. 16, pp. 3643–3658, 2003, doi: 10.1016/S0009-2509(03)00223-9.

[90] M. R. Rahimpour, J. Fathikalajahi, B. Moghtaderi, and A. N. Farahani, "A grade transition strategy for the prevention of melting and agglomeration of particles in an ethylene polymerization reactor," *Chem. Eng. Technol.*, vol. 28, no. 7, pp. 831–841, 2005, doi: 10.1002/ceat.200500055.

[91] C. Chatzidoukas, V. Kanellopoulos, and C. Kiparissides, "On the production of polyolefins with bimodal molecular weight and copolymer composition distributions in catalytic gas-phase fluidized-bed reactors," *Macromol. Theory Simulations*, vol. 16, no. 8, pp. 755–769, 2007, doi: 10.1002/mats.200700033.

[92] A. Farhangiyan Kashani, H. Abedini, and M. R. Kalaee, "Simulation of an Industrial Linear Low Density Polyethylene Plant," *Chem. Prod. Process Model.*, vol. 6, no. 1, p. 34, 2011, doi: 10.2202/1934-2659.1611.

[93] G. Dompazis, A. Roussos, V. Kanellopoulos, and C. Kiparissides, "Dynamic evolution of the particle size distribution in multistage olefin polymerization reactors," *Comput. Aided Chem. Eng.*, vol. 20, no. C, pp. 427–432, 2005, doi: 10.1016/S1570-7946(05)80193-2.

[94] R. Jafari, R. Sotudeh-Gharebagh, and N. Mostoufi, "Modular simulation of fluidized bed reactors," *Chem. Eng. Technol.*, vol. 27, no. 2, pp. 123–129, 2004, doi: 10.1002/ceat.200401908.

[95] M. Alizadeh, N. Mostoufi, S. Pourmahdian, and R. Sotudeh-Gharebagh, "Modeling of fluidized bed reactor of ethylene polymerization," *Chem. Eng. J.*, vol. 97, no. 1, pp. 27–35,

2004, doi: 10.1016/S1385-8947(03)00133-5.

[96]   H. Cui, N. Mostoufi, and J. Chaouki, "Characterization of dynamic gas-solid distribution in fluidized beds," *Chem. Eng. J.*, vol. 79, no. 2, pp. 133–143, 2000, doi: 10.1016/S1385-8947(00)00178-9.

[97]   N. Mostoufi, H. Cui, and J. Chaouki, "A comparison of two- and single-phase models for fluidized-bed reactors," in *Industrial and Engineering Chemistry Research*, 2001, vol. 40, no. 23, pp. 5526–5532, doi: 10.1021/ie010121n.

[98]   A. R. Abrahamsen and D. Geldart, "Behaviour of gas-fluidized beds of fine powders part II. Voidage of the dense phase in bubbling beds," *Powder Technol.*, vol. 26, no. 1, pp. 47–55, 1980, doi: 10.1016/0032-5910(80)85006-6.

[99]   J. Chaouki, A. Gonzalez, C. Guy, and D. Klvana, "Two-phase model for a catalytic turbulent fluidized-bed reactor: Application to ethylene synthesis," *Chem. Eng. Sci.*, vol. 54, no. 13–14, pp. 2039–2045, 1999, doi: 10.1016/S0009-2509(98)00438-2.

[100] A. Shamiri, M. A. Hussain, F. S. Mjalli, M. S. Shafeeyan, and N. Mostoufi, "Experimental and modeling analysis of propylene polymerization in a pilot-scale fluidized bed reactor," *Ind. Eng. Chem. Res.*, vol. 53, no. 21, pp. 8694–8705, 2014, doi: 10.1021/ie501155h.

[101] K. Y. Choi and W. Harmon Ray, "The dynamic behaviour of fluidized bed reactors for solid catalysed gas phase olefin polymerization," *Chem. Eng. Sci.*, vol. 40, no. 12, pp. 2261–2279, Jan. 1985, doi: 10.1016/0009-2509(85)85128-9.

[102] H. Hatzantonis, H. Yiannoulakis, A. Yiagopoulos, and C. Kiparissides, "Recent developments in modeling gas-phase catalyzed olefin polymerization fluidized-bed reactors: The effect of bubble size variation on the reactor's performance," *Chem. Eng. Sci.*, vol. 55, no. 16, pp. 3237–3259, Aug. 2000, doi: 10.1016/S0009-2509(99)00565-5.

[103] M. R. Abbasi, A. Shamiri, and M. A. Hussain, "Dynamic modeling and Molecular Weight Distribution of ethylene copolymerization in an industrial gas-phase Fluidized-Bed Reactor," *Adv. Powder Technol.*, vol. 27, no. 4, pp. 1526–1538, Jul. 2016, doi: 10.1016/j.apt.2016.05.014.

[104] A. Lucas, J. Arnaldos, J. Casal, and L. Pulgjaner, "Improved Equation for the Calculation of Minimum Fluidization Velocity," *Ind. Eng. Chem. Process Des. Dev.*, vol. 25, no. 2, pp. 426–429, 1986, doi: 10.1021/i200033a013.

[105] C. - Y Shiau and C. - J Lin, "Equation for the superficial bubble- phase gas velocity in

fluidized beds," *AIChE J.*, vol. 37, no. 6, pp. 953–954, Jun. 1991, doi: 10.1002/aic.690370619.

[106] J. Davidson and D. Harrison, *Fluidized particles*. Cambridge University Press, 1963.

[107] D. B. Bukur, C. V. Wittmann, and N. R. Amundson, "Analysis of a model for a nonisothermal continuous fluidized bed catalytic reactor," *Chem. Eng. Sci.*, vol. 29, no. 5, pp. 1173–1192, May 1974, doi: 10.1016/0009-2509(74)80117-X.

[108] S. Mori and C. Y. Wen, "Estimation of bubble diameter in gaseous fluidized beds," *AIChE J.*, vol. 21, no. 1, pp. 109–115, Jan. 1975, doi: 10.1002/aic.690210114.

[109] K. Hillegardt and J. Werther, "Local bubble gas hold-up and expansion of gas/solid fluidized beds," *Ger. Chem. Eng.*, vol. 9, pp. 215–221, 1986.

[110] M. Horio and A. Nonaka, "A generalized bubble diameter correlation for gas- solid fluidized beds," *AIChE J.*, vol. 33, no. 11, pp. 1865–1872, Nov. 1987, doi: 10.1002/aic.690331113.

[111] T. E. Broadhurst and H. A. Becker, "Onset of fluidization and slugging in beds of uniform particles," *AIChE J.*, vol. 21, no. 2, pp. 238–247, Mar. 1975, doi: 10.1002/aic.690210204.

[112] S. P. Sit and J. R. Grace, "Effect of bubble interaction on interphase mass transfer in gas fluidized beds," *Chem. Eng. Sci.*, vol. 36, no. 2, pp. 327–335, Jan. 1981, doi: 10.1016/0009-2509(81)85012-9.

[113] M. H. Peters, L. S. Fan, and T. L. Sweeney, "Reactant dynamics in catalytic fluidized bed reactors with flow reversal of gas in the emulsion phaset," *Chem. Eng. Sci.*, vol. 37, no. 4, pp. 553–565, Jan. 1982, doi: 10.1016/0009-2509(82)80118-8.

[114] A. Mirzaei, A. Kiashemshaki, and M. Emanmi, "Fluidized Bed Polyethylene Reactor Modeling in Condensed Mode Operation," *Macromol. Symp.*, vol. 259, no. 1, pp. 135–144, 2007.

[115] Y. Zhou, J. Wang, Y. Yang, and W. Wu, "Modeling of the Temperature Profile in an Ethylene Polymerization Fluidized-Bed Reactor in Condensed-Mode Operation," *Ind. Eng. Chem. Res.*, vol. 52, no. 12, p. 4455−4464, 2013.

[116] F. A. N. Fernandes and L. M. F. Lona Batista, "Fluidized-bed reactor and physicalchemical properties modeling for polyethylene production," in *Computers and Chemical Engineering*, Jun. 1999, vol. 23, no. SUPPL. 1, doi: 10.1016/S0098-1354(99)80197-5.

[117] F. A.N. Fernandes and L. M.F. Lona, "Heterogeneous modeling for fluidized-bed polymerization reactor," *Chem. Eng. Sci.*, vol. 56, no. 3, pp. 963–969, 2001, doi: 10.1016/S0009-2509(00)00311-0.

[118] F. A. N. Fernandes and L. M. F. Lona, "Heterogeneous modeling of fluidized bed polymerization reactors. Influence of mass diffusion into the polymer particle," *Comput. Chem. Eng.*, vol. 26, no. 6, pp. 841–848, 2002, doi: 10.1016/S0098-1354(02)00010-8.

[119] A. S. Ibrehem, M. A. Hussain, and N. M. Ghasem, "Modified mathematical model for gas phase olefin polymerization in fluidized-bed catalytic reactor," *Chem. Eng. J.*, vol. 149, no. 1–3, pp. 353–362, 2009, doi: 10.1016/j.cej.2008.05.014.

[120] W. E. Grosso and M. G. Chiovetta, "Modeling a fluidized-bed reactor for the catalytic polimerization of ethylene: particle size distribution effects," *Lat. Am. Appl. Res.*, vol. 35, no. 1, pp. 67–76, 2005, Accessed: Apr. 10, 2019. [Online]. Available: http://www.scielo.org.ar/pdf/laar/v35n1/v35n1a10.pdf.

[121] X. Fan *et al.*, "Thermal-Stability Analysis of Ethylene-Polymerization Fluidized-Bed Reactors under Condensed-Mode Operation through a TPM-PBM Integrated Model," *Ind. Eng. Chem. Res.*, vol. 58, no. 22, pp. 9486–9499, 2019, doi: 10.1021/acs.iecr.9b00071.

[122] K. B. McAuley, J. P. Talbot, and T. J. Harris, "A comparison of two-phase and well-mixed models for fluidized-bed polyethylene reactors," *Chem. Eng. Sci.*, vol. 49, no. 13, pp. 2035–2045, 1994.

[123] K. Kato and C. Y. Wen, "Bubble assemblage model for fluidized bed catalytic reactors," *Chem. Eng. Sci.*, vol. 24, no. 8, pp. 1351–1369, 1969, doi: 10.1016/0009-2509(69)85055-4.

[124] P. N. Rowe, "Prediction of bubble size in a gas fluidised bed," *Chem. Eng. Sci.*, vol. 31, no. 4, pp. 285–288, Jan. 1976, doi: 10.1016/0009-2509(76)85073-7.

[125] J. H. Choi, J. E. Son, and S. D. Kim, "Generalized model for bubble size and frequency in gas-fluidized beds," *Ind. Eng. Chem. Res.*, vol. 37, no. 6, pp. 2559–2564, 1998, doi: 10.1021/ie970915v.

[126] C. Y. Shiau and C. J. Lin, "An improved bubble assemblage model for fluidized-bed catalytic reactors," *Chem. Eng. Sci.*, vol. 48, no. 7, pp. 1299–1308, Apr. 1993, doi: 10.1016/0009-2509(93)81010-S.

[127] J. R. Grace, "Modelling and Simulation of Two-Phase Fluidized Bed Reactors," in

Chemical Reactor Design and Technology, Springer Netherlands, 1986, pp. 245–289.

[128] O. Ashrafi, N. Mostoufi, and R. Sotudeh-Gharebagh, "Two phase steady-state particle size distribution in a gas-phase fluidized bed ethylene polymerization reactor," *Chem. Eng. Sci.*, vol. 73, pp. 1–7, 2012, doi: 10.1016/j.ces.2012.01.018.

[129] A. Kiashemshaki, N. Mostoufi, and R. Sotudeh-Gharebagh, "Two-phase modeling of a gas phase polyethylene fluidized bed reactor," *Chem. Eng. Sci.*, vol. 61, no. 12, pp. 3997–4006, 2006, doi: 10.1016/j.ces.2006.01.042.

[130] G. Dompazis, V. Kanellopoulos, V. Touloupides, and C. Kiparissides, "Development of a multi-scale, multi-phase, multi-zone dynamic model for the prediction of particle segregation in catalytic olefin polymerization FBRs," *Chem. Eng. Sci.*, vol. 63, no. 19, pp. 4735–4753, 2008, doi: 10.1016/j.ces.2007.08.069.

[131] J. Y. Kim and K. Y. Choi, "Modeling of particle segregation phenomena in a gas phase fluidized bed olefin polymerization reactor," *Chem. Eng. Sci.*, vol. 56, no. 13, pp. 4069–4083, 2001, doi: 10.1016/S0009-2509(01)00078-1.

[132] Y. H. Farid, H. A. Farag, M. E. Ossman, and M. S. Mansour, "Development of mathematical model for a polyethylene fluidized bed reactor," *IRACST - Eng. Sci. Technol. An Int. J.*, vol. 2, no. 5, pp. 935–944, 2012.

[133] H. Farag, M. Ossman, M. Mansour, and Y. Farid, "Modeling of fluidized bed reactor for ethylene polymerization: effect of parameters on the single-pass ethylene conversion," *Int. J. Ind. Chem.*, vol. 4, no. 1, p. 20, 2013, doi: 10.1186/2228-5547-4-20.

[134] M. J. H. Khan, M. A. Hussain, Z. Mansourpour, N. Mostoufi, N. M. Ghasem, and E. C. Abdullah, "CFD simulation of fluidized bed reactors for polyolefin production - A review," *Journal of Industrial and Engineering Chemistry*, vol. 20, no. 6. pp. 3919–3946, 2014, doi: 10.1016/j.jiec.2014.01.044.

[135] J. Jung, D. Gidaspow, and I. K. Gamwo, *Design and understanding of fluidized-bed reactors : application of CFD techniques to multiphase flows*. VDM Verlag Dr. Müller, 2009.

[136] J. Ding and D. Gidaspow, "A bubbling fluidization model using kinetic theory of granular flow," *AIChE J.*, vol. 36, no. 4, pp. 523–538, Apr. 1990, doi: 10.1002/aic.690360404.

[137] D. L. Marchisio, J. T. Pikturna, R. O. Fox, R. D. Vigil, and A. A. Barresi, "Quadrature method of moments for population-balance equations," *AIChE Journal*, vol. 49, no. 5.

John Wiley & Sons, Ltd, pp. 1266–1276, May 01, 2003, doi: 10.1002/aic.690490517.

[138] D. L. Marchisio, R. D. Vigil, and R. O. Fox, "Implementation of the quadrature method of moments in CFD codes for aggregation - breakage problems," *Chem. Eng. Sci.*, vol. 58, no. 15, pp. 3337–3351, Aug. 2003, doi: 10.1016/S0009-2509(03)00211-2.

[139] D. L. Marchisio, R. D. Vigil, and R. O. Fox, "Quadrature method of moments for aggregation-breakage processes," *J. Colloid Interface Sci.*, vol. 258, no. 2, pp. 322–334, Feb. 2003, doi: 10.1016/S0021-9797(02)00054-1.

[140] D. L. Marchisio, R. O. Fox, and R. O. Fox, *Computational models for polydisperse particulate and multiphase systems*. Cambridge University Press, 2010.

[141] H. Neau *et al.*, "Massively parallel numerical simulation using up to 36,000 CPU cores of an industrial-scale polydispersed reactive pressurized fluidized bed with a mesh of one billion cells," *Powder Technol.*, vol. 366, pp. 906–924, Apr. 2020, doi: 10.1016/j.powtec.2020.03.010.

[142] V. Akbari, T. N. G. Borhani, A. Shamiri, R. Aramesh, M. A. Hussain, and M. K. A. Hamid, "2D CFD-PBM simulation of hydrodynamic and particle growth in an industrial gas phase fluidized bed polymerization reactor," *Chem. Eng. Res. Des.*, vol. 104, pp. 53–67, Dec. 2015, doi: 10.1016/j.cherd.2015.07.016.

[143] V. Akbari, T. Nejad Ghaffar Borhani, A. Shamiri, and M. Kamaruddin Abd. Hamid, "A CFD-PBM coupled model of hydrodynamics and mixing/segregation in an industrial gas-phase polymerization reactor," *Chem. Eng. Res. Des.*, vol. 96, pp. 103–120, Apr. 2015, doi: 10.1016/j.cherd.2015.02.007.

[144] Y. Che *et al.*, "A CFD-PBM model considering ethylene polymerization for the flow behaviors and particle size distribution of polyethylene in a pilot-plant fluidized bed reactor," *Powder Technol.*, vol. 286, pp. 107–123, Dec. 2015, doi: 10.1016/j.powtec.2015.07.049.

[145] Y. Che *et al.*, "CFD prediction of scale-up effect on the hydrodynamic behaviors of a pilot-plant fluidized bed reactor and preliminary exploration of its application for non-pelletizing polyethylene process," *Powder Technol.*, vol. 278, pp. 94–110, 2015, doi: 10.1016/j.powtec.2015.02.022.

[146] Y. Che *et al.*, "An Insight into the Temperature Field and Particle Flow Patterns in a Fluidized Bed Reactor for Nonpelletizing Polyethylene Process Using a 3D CFD-PBM

Model," *Ind. Eng. Chem. Res.*, vol. 55, no. 30, pp. 8258–8270, Aug. 2016, doi: 10.1021/acs.iecr.6b00596.

[147] Z. Zou *et al.*, "Numerical analysis of residence time distribution of solids in a bubbling fluidized bed based on the modified structure-based drag model," *Particuology*, vol. 32, pp. 30–38, Jun. 2017, doi: 10.1016/j.partic.2016.09.005.

[148] Z. Zou *et al.*, "Hydrodynamic and solids residence time distribution in a binary bubbling fluidized bed: 3D computational study coupled with the structure-based drag model," *Chem. Eng. J.*, vol. 321, pp. 184–194, Aug. 2017, doi: 10.1016/j.cej.2017.03.110.

[149] M. J. H. Khan, M. A. Hussain, and I. M. Mujtaba, *Multiphasic reaction modeling for polypropylene production in a pilot-scale catalytic reactor*, vol. 8, no. 6. 2016.

[150] P. Bumphenkiattikul, S. Limtrakul, T. Vatanatham, P. Khongprom, and P. A. Ramachandran, "Heat transfer effect in scaling-up a fluidized bed reactor for propylene polymerization," *RSC Adv.*, vol. 8, no. 50, pp. 28293–28312, Aug. 2018, doi: 10.1039/c8ra04834g.

[151] S. Schneiderbauer, S. Puttinger, S. Pirker, P. Aguayo, and V. Kanellopoulos, "CFD modeling and simulation of industrial scale olefin polymerization fluidized bed reactors," *Chem. Eng. J.*, vol. 264, pp. 99–112, 2015, doi: 10.1016/j.cej.2014.11.058.

[152] Y. Yao, Y. J. He, Z. H. Luo, and L. Shi, "3D CFD-PBM modeling of the gas-solid flow field in a polydisperse polymerization FBR: The effect of drag model," *Adv. Powder Technol.*, vol. 25, no. 5, pp. 1474–1482, Sep. 2014, doi: 10.1016/j.apt.2014.04.001.

[153] Y. Yao, J. W. Su, and Z. H. Luo, "CFD-PBM modeling polydisperse polymerization FBRs with simultaneous particle growth and aggregation: The effect of the method of moments," *Powder Technol.*, vol. 272, pp. 142–152, Mar. 2015, doi: 10.1016/j.powtec.2014.11.037.

[154] Y. Tian and P. Mehrani, "Effect of particle size in fluidization of polyethylene particle mixtures on the extent of bed electrification and wall coating," *J. Electrostat.*, vol. 76, pp. 138–144, Aug. 2015, doi: 10.1016/j.elstat.2015.05.020.

[155] R. G. Rokkam, A. Sowinski, R. O. Fox, P. Mehrani, and M. E. Muhle, "Computational and experimental study of electrostatics in gas-solid polymerization fluidized beds," *Chem. Eng. Sci.*, vol. 92, pp. 146–156, 2013, doi: 10.1016/j.ces.2013.01.023.

[156] M. Ray, F. Chowdhury, A. Sowinski, P. Mehrani, and A. Passalacqua, "An Euler-Euler model for mono-dispersed gas-particle flows incorporating electrostatic charging due to

particle-wall and particle-particle collisions," *Chem. Eng. Sci.*, vol. 197, pp. 327–344, 2019, doi: 10.1016/j.ces.2018.12.028.

[157] H. Pan, X. F. Liang, and Z. H. Luo, "CFD modeling of the gas–solid two-fluid flow in polyethylene FBRs: From traditional operation to super-condensed mode," *Adv. Powder Technol.*, vol. 27, no. 4, pp. 1494–1505, Jul. 2016, doi: 10.1016/j.apt.2016.05.011.

[158] H. Pan, X. F. Liang, L. T. Zhu, and Z. H. Luo, "Important Analysis of Liquid Vaporization Modeling Scheme in Computational Fluid Dynamics Modeling of Gas-Liquid-Solid Polyethylene Fluidized Bed Reactors," *Ind. Eng. Chem. Res.*, vol. 56, no. 36, pp. 10199– 10213, Sep. 2017, doi: 10.1021/acs.iecr.7b02912.

[159] H. Pan, Q. Liu, and Z. H. Luo, "Modeling and simulation of particle size distribution behavior in gas–liquid–solid polyethylene fluidized bed reactors," *Powder Technol.*, vol. 328, pp. 95–107, 2018, doi: 10.1016/j.powtec.2018.01.014.

[160] P. Hui, L. Yuan-Xing, and L. Zheng-Hong, "Computational fluid dynamics simulation of gas–liquid–solid polyethylene fluidized bed reactors incorporating with a dynamic polymerization kinetic model," *Asia-Pacific J. Chem. Eng.*, vol. 14, no. 1, p. e2265, Jan. 2019, doi: 10.1002/apj.2265.